

International Journal of Modern Physics D
 © World Scientific Publishing Company

e^\pm Excesses in the Cosmic Ray Spectrum and Possible Interpretations

Yi-Zhong Fan

*Department of Physics and Astronomy, University of Nevada, Las Vegas, NV 89119, USA;
 Purple Mountain Observatory, Chinese Academy of Sciences, 210008, Nanjing, China*

Bing Zhang

Department of Physics and Astronomy, University of Nevada, Las Vegas, NV 89119, USA

Jin Chang

Purple Mountain Observatory, Chinese Academy of Sciences, 210008, Nanjing, China

Received Day Month Year

Revised Day Month Year

Communicated by Managing Editor

The data collected by ATIC, PPB-BETS, FERMI-LAT and HESS all indicate that there is an electron/positron excess in the cosmic ray energy spectrum above ~ 100 GeV, although different instrumental teams do not agree on the detailed spectral shape. PAMELA also reported a clear excess feature of the positron fraction above several GeV, but no excess in anti-protons. Here we review the observational status and theoretical models of this interesting observational feature. We pay special attention to various physical interpretations proposed in the literature, including modified supernova remnant models for the e^\pm background, new astrophysical sources, and new physics (the dark matter models). We suggest that although most models can make a case to interpret the data, with the current observational constraints the dark matter interpretations, especially those invoking annihilation, require much more exotic assumptions than some astrophysical interpretations. Future observations may present some “smoking-gun” observational tests to differentiate among different models and to identify the correct interpretation to the phenomenon.

Keywords: e^\pm excess, Supernova remnants, Pulsar, Dark matter, Particle

1. Introduction

Cosmic rays (CRs) are energetic particles originating from outer space that impinge on Earth’s atmosphere. Almost 90% of all the incoming cosmic ray particles are protons, about 10% are helium nuclei (alpha particles), and slightly under 1% are heavier elements and electrons¹. The history of the CR studies may be rooted in 1901 when two groups came to the same conclusion that pure air in a closed vessel possessed some electrical conductivity^{2,3}, while no visible sources of air ionization were observed. At that time it was already known that X-rays and radioactivity were factors contributing to the enhanced electrical conductivity of gases. Therefore, the

observed effect of “dark current” caused by residual ionization of the air, was then regarded as being associated with radioactive contamination both in the air and in the environment¹. Wilson speculated that the residual ionization was due to certain highly penetrating radiation coming from outside the Earth’s atmosphere⁴. Such a speculation was convincingly confirmed by Hess⁵ and Kolhorster⁶ about 10 years later. August 7, 1912, the date of Hess’ most successful balloon flight among the total of ten, is generally regarded as the date of the discovery of cosmic rays. The discovery of cosmic rays opens a new window not only for high energy astrophysics but also for high energy physics. This is because prior to the constructions of modern particle accelerators, high energy particles could only be observed in cosmic rays. Between 1932 and 1953, many new particles, including positrons, μ^\pm -leptons, π^\pm -mesons, K^+ - and K^0 -mesons, Λ^0 -, Ξ^- - and Σ^+ -hyperons, were all discovered in use of cosmic rays (Ref.1 and the references therein).

A thorough review of CRs can be found in many excellent articles and books^{7,8,9,10}, and is beyond the scope of this review. Here we will focus on a small fraction of these high energy particles, the electron/positron (e^\pm) CRs. Although CRs had been discovered in 1912, CR electrons reaching the earth at energies above a few hundred MeV had not been convincingly identified until 1961^{11,12}. The first positron-to-electron ratio in CRs up to an energy ~ 1 GeV was later reported in 1964¹³. Most CR electrons are likely from the supernova remnants while the CR positrons are mainly produced through hadronic processes when CR protons collide with intergalactic hydrogen. In such a scenario there should be no prominent feature in the TeV energies in the electron/positron total spectrum, and the positron-to-electron ratio $\mathcal{R} \equiv \Phi_{e^+}/(\Phi_{e^+} + \Phi_{e^-})$ should drop with energy monotonously¹⁴. A rise of the positron-to-electron ratio above ~ 10 GeV was observed in 1974^{15a}. Such a tendency was confirmed by several balloon flights, including the 1976 flight by the New Mexico State University group launched from Palestine, Texa in 1976²⁰, and 1984 flight by the University of Chicago group launched from Hawaii¹⁹, and in particular, by the recent PAMELA mission^{21,22} (see section 2 for extensive discussion). In 1987 it was already clear that the rising behavior of \mathcal{R} above ~ 10 GeV is not predicted by calculations of CR propagation^{19,23} and may imply an excess of CR positrons. Recently, ATIC²⁴, PPB-BETS²⁵ and Fermi-LAT²⁶ reported electron/positron total spectrum up to TeV and found a hardening/bump in the energy range from 100 GeV to 1 TeV. In the conventional approach, the injection spectrum of the electrons (positrons) is taken as a single power-law. Since diffusion and electron/positron cooling are more efficient in higher energies, one would expect that the spectrum should soften with energy. Therefore the unexpected spectrum hardening observed by these detectors strongly suggest another excess (besides the positron

^aIn 1965, a group reported $\mathcal{R} \sim 0.8$ at 10 – 30 GeV, implying an excess of positron CRs¹⁶. It was however only based on a total of 13 events and therefore highly uncertain¹⁷. If one plots the single data of Ref.18 (at ~ 10 GeV) published in 1969 together with some other data at lower energies reported before, one would also get a positron excess¹⁹.

fraction excess). Interestingly this total e^\pm excess is consistent with extrapolating the positron fraction excess to high energies. These interesting features draw a lot of attention, and various physical origins have been explored. In the literature, new astrophysical sources or even new physics (dark matter) are widely suggested. Some more conservative authors argue that the excesses are simply due to inadequate accounts on the electron/positron CR background in previous modeling. The situation is unclear. Several reviews appeared recently but are mainly focused on dark matter models^{27,28}. In this review we plan to present a more complete overview of this interesting observational feature and various physical interpretations.

The structure of this review is as follows. We first discuss the observational aspects of the e^\pm excesses in Section 2. We then review the cosmic ray propagation models and the general cosmic sources of e^\pm in Section 3. In the next three sections (4-6), we discuss three proposed physical origins of the observed e^\pm excess, including the modified supernova remnant (SNR) models of e^\pm background, new astrophysical sources, and new physics. We summarize the strengths/weaknesses of various models in Section 7 with a commentary on the prospects.

2. Observations

Different from the CR protons/nuclei, the TeV electrons/positrons suffer significant energy loss and cannot reach us if the source is not nearby (i.e., ≤ 1 kpc). Accurate measurements of the high-energy electron/positron CRs then provide a unique opportunity to probe the origin and propagation of CRs in the local interstellar medium and to constrain models of the diffuse gamma-ray emission. Observations of electrons have been notoriously difficult because of their low intensity requiring, in particular at high energies, rather large detectors, and because of the need of effective discrimination against proton-induced background. So far the high-energy electron spectrum was measured by some balloon-borne experiments (in addition to those already mentioned in the introduction, some others can be found in Refs. 29, 30, 31, 32, 33, 34, 35, 36, 37, 38), some space missions (including IMP-1³⁹, IMP-III⁴⁰, IMP-IV⁴¹, IMP-7⁴², AMS-01⁴³, PAMELA²¹ and Fermi²⁶), and the ground-based Cherenkov telescope H.E.S.S.⁴⁴.

2.1. Experiments

2.1.1. Balloon-borne experiments

We first briefly review the development of technology used in the experiments. In two of the very early Balloon-borne experiments^{29,11}, the cloud chamber technology was employed, which was soon abandoned with the introduction of other more sophisticated detectors, both visible and electronic (see Ref.17 for a review on the development of technology in the early experiments). In the two flights at Fort Churchill in 1963¹³, the spark chamber technique was adopted. With the help of one permanent magnet, electrons and positrons were distinguished. Such an instru-

ment was later improved³¹, through replacing the liquid Cerenkov detector by a gas Cerenkov detector to enable the determination of the momentum and charge of electrons up to 5–10 GeV. A group from Bombay^{16,45} adopted the nuclear emulsion stack technique, which measures CR electrons to an energy above 50 GeV. In order to identify electron showers efficiently, multiple pulse-height analyses of many counters and time of flight techniques had been used in 3 high-latitude balloon flights from Palestine, Texas in 1970 by the Chicago group⁴⁶. Later they added a transition radiation detector, consisting of a sandwich of six radiators and six multiwire proportional chambers, to improve electron and positron discrimination^{47,48}. In a balloon-borne magnetic spectrometer experiment^{15,49}, a super-conducting magnetic spectrometer was adopted, and a new bremsstrahlung-identification technique was developed to measure the separate e^- and e^+ spectrum in the primary CRs from 4 to 50 GeV. The emulsion chamber technique was used to detect CR electrons to an energy above 1 TeV^{50,51}. In the experiment of Balloon-borne Electron Telescope with Scintillating Fibers (BETS), the absolute energy spectrum of electrons was measured with a highly granulated fiber calorimeter³⁸. Finally the Advanced Thin Ionization Calorimeter (ATIC) experiments used an ionization calorimeter to measure the energy deposited by cascades formed by particles interacting in a thick carbon target²⁴.

Since 1950, dozens of balloon-born experiments dedicated to electron/positron CR observations have been carried out. Below we only mention some recent ones that are most relevant to the main topic of this review, the electron/positron excess.

Two early charge determining experiments. The Chicago group firstly used a permanent magnet to measure the positron-to-electron ratio. In the energy range $0.2 \text{ GeV} < \mathcal{E} < 10 \text{ GeV}$, the ratio \mathcal{R} was found to decrease with energy³². Adopting a super-conducting magnetic spectrometer, \mathcal{R} was measured from 5 GeV to 50 GeV¹⁵. Although scatter is large, an tendency of increasing \mathcal{R} for $\mathcal{E} > 10 \text{ GeV}$ is present. Such a behavior was confirmed by some subsequent groups (e.g. Ref. 19, 20), but not by some others.

The emulsion chamber experiments by a Japanese group started in 1968. The $e^+ + e^-$ spectrum derived by combining data from the chambers exposed from 1968 to 1976 was well represented by $J(\mathcal{E}) = 1.6 \times 10^{-4} (\mathcal{E}/100 \text{ GeV})^{-3.3 \pm 0.2} \text{ m}^{-2} \text{ sr}^{-1} \text{ s}^{-1} \text{ GeV}^{-1}$ in the energy range of $30 - 10^3 \text{ GeV}$ ⁵⁰, which is steeper than the spectrum $J \propto \mathcal{E}^{-2.61 \pm 0.1}$ obtained in the early nuclear emulsion stack experiment by the Bombay group⁵². This confirms some early results, for example, obtained with an ionization calorimeter^{53,54}. The observations in 1996 and 1998 extended the $e^+ + e^-$ spectrum to $\sim 2 \text{ TeV}$ ⁵¹ and might suggest a steepening above 1 TeV.

High-Energy Antimatter Telescope (HEAT) is a NASA-supported program of high-altitude balloon-borne experiments to study antimatter in the primary cosmic radiation. The HEAT detector³⁶ consists of a magnetic spectrometer combined with a transition radiation detector, an electromagnetic calorimeter, and

time-of-flight scintillators. It can measure the cosmic-ray positron fraction from 1 to 50 GeV. A new version of the HEAT instrument, HEAT-pbar was designed to observe the high-energy cosmic-ray antiproton flux but it is also suited for the observation of electrons and positrons at energies below 15 GeV⁵⁵. The combined data from the three HEAT flights indicate a small positron flux of nonstandard origin above 5 GeV⁵⁵. The evidence for the tendency of increasing \mathcal{R} for $\mathcal{E} > 10$ GeV is however rather weak, consistent with what was found in the Cosmic AntiParticle Ring Imaging Cherenkov Experiment in 1998⁵⁶.

BETS and PPB-BETS. BETS represents a detector, the Balloon-borne Electron Telescope with Scintillating fibers, which preserves the superior qualities of both electronic detectors and emulsion chambers³⁸. With such a balloon-borne payload, cosmic-ray electrons were observed in the energy range from 12 to ~ 100 GeV. The energy spectrum is described by a power-law index of -3.00 ± 0.09 , and the absolute differential intensity at 10 GeV is $0.199 \pm 0.015 \text{ m}^{-2} \text{ s}^{-1} \text{ sr}^{-1} \text{ GeV}^{-1.38}$. PPB-BETS is an advanced version of BETS measuring the electron spectrum up to TeV and was flown by Polar Patrol Balloon (PPB) in Antarctica. The results from the PPB-BETS calorimeter indicates a possible hump in the energy range 100 GeV to 1 TeV in the total spectrum²⁵, consistent with that reported by ATIC (see below).

The Advanced Thin Ionization Calorimeter (ATIC) is a balloon-borne instrument flying in the stratosphere over Antarctica to measure the energy and composition of cosmic rays. ATIC was launched from the McMurdo Station for the first time in December 2000 and has since completed three successful flights out of four. The detector uses the principle of ionization calorimetry: several layers of the scintillator bismuth germanate emit light as they are struck by particles, allowing to calculate the particles' energy. A silicon matrix is used to determine the particles' electrical charge²⁴. The main discovery is a spike-like $e^+ + e^-$ spectrum feature in the energy range of 300 – 800 GeV²⁴.

2.1.2. Space station and satellite experiments

The series of Interplanetary Monitoring Platform (IMP) experiments measure the low energy electron CRs ($\mathcal{E} < 1$ GeV), which are not the focus of this review. In the following we only focus on several relevant missions.

AMS-01 (Alpha Magnetic Spectrometer - 01) is the predecessor to AMS-02, a detector to be operated on the International Space Station (ISS) for at least 3 years (<http://ams.cern.ch/>). The AMS-01 experiment was flown on the Space Shuttle Discovery for ten days in June, 1998. It was designed to search for various types of unusual matter by measuring cosmic rays. The detector consisted of a permanent Nd-Fe-B magnet, six silicon tracker planes, an anticoincidence scintillator counter system, the time-of-flight (TOF) system consisting of four layers of scintillator counters and a threshold aerogel Cerenkov detector. With these instruments, the high-energy proton, electron, positron, helium, antiproton and deuterium spec-

tra were accurately measured. The obtained \mathcal{R} in the energy range of 1 – 30 GeV is largely consistent with that obtained by HEAT⁴³.

PAMELA, the Payload for Antimatter Matter Exploration and Light-nuclei Astrophysics, is a powerful particle identifier using a permanent magnet spectrometer with a variety of specialized detectors (<http://pamela.roma2.infn.it/index.php>). It is measuring with unprecedented precision and sensitivity the abundance and energy spectra of CR electrons, positrons, antiprotons and light nuclei over a very large range of energy from 50 MeV to hundreds GeV, depending on the species^{21,57}. The most exciting discovery made so far is the unambiguous detection of the increasing behavior of \mathcal{R} in the energy range 10 – 100 GeV^{21,22}.

Fermi γ -ray Space Telescope is an international and multi-agency space mission that studies the cosmos in the energy range 10 keV - 300 GeV (<http://fermi.gsfc.nasa.gov/>). The Large Area Telescope (LAT) is the main instrument on-board. Conceived as a multipurpose observatory to survey the variable gamma-ray sky between 20 MeV and 300 GeV including the largely unexplored energy window above 10 GeV, it is designed as a low aspect ratio, large area pair conversion telescope to maximize its field of view and effective area. The LAT angular, energy and timing resolutions rely on modern solid state detectors and electronics. Since electromagnetic cascades are germane to both electron and photon interactions in matter, the LAT is also by its nature a detector for electrons and positrons²⁶. The measurement of the CR electron spectrum from 20 GeV to 1 TeV based on the first half year data also displays a spectrum hump in the 100 – 1000 GeV range, although the signature is not as prominent as that found by ATIC and PPB-BETS.

2.1.3. *Ground-based telescopes*

H.E.S.S., the High Energy Stereoscopic System, is an array of four imaging atmospheric Cherenkov telescopes located in the Khomas Highland of Namibia (<http://www.mpi-hd.mpg.de/hfm/HESS/>). It is designed to obtain the Cherenkov images of cosmic-ray hadrons and electrons, as well as gamma-ray photons (sorted according to the relative flux). To measure the spectrum of electrons, the other two components (hereafter background events) have to be eliminated. First, data taken from the sky regions known to contain gamma-ray sources are rejected. However, the most critical aspect of the electron analysis is the efficient rejection of the hadronic background. A Random Forest approach was used to convert the image information into a single parameter describing the degree to which a shower is electron-like, that spans from 0 (for hadrons) to 1 (for electrons). By Monte-Carlo simulations, the distribution of this parameter for simulated hadrons and electrons is determined (See Figure 1 in Aharonian et al.⁴⁴). The number of measured electron showers in each energy band can then be deduced. In this way, the spectrum is measured from 0.35 - 4 TeV. While the overall electron flux measured by H.E.S.S. is consistent with the ATIC data within statistical and systematic errors, the H.E.S.S. data do

not confirm a pronounced peak in the electron spectrum suggested by ATIC and PPB-BETS⁵⁸.

2.2. Observation results

Prior to 2008, the high energy $e^+ + e^-$ data are consistent with a featureless power-law spectrum within errors, which is in agreement with the theoretical predictions from both analytical and numerical models¹⁴. Recently, the ATIC balloon experiment²⁴ discovered a prominent spectral feature at around 600 GeV in the $e^+ + e^-$ spectrum. Instead of a decaying feature expected by electron/positron cooling, the team discovered a clear excess of the $e^+ + e^-$ in the energy range of $\sim 300 - 800$ GeV. Such a feature was also marginally observed by PPB-BETS²⁵. Furthermore, H.E.S.S. reported a significant steepening of the electron spectrum above ~ 1 TeV^{44,58}. The Fermi-LAT Collaboration later reported a high-precision measurement of the $e^+ + e^-$ spectrum from 20 GeV to 1 TeV²⁶. As shown in Fig.1, their measured $e^+ + e^-$ spectrum may be fitted by a single power-law $J = (175.40 \pm 6.09)\varepsilon^{-(3.045 \pm 0.008)} \text{ GeV}^{-1} \text{ m}^{-2} \text{ s}^{-1} \text{ sr}^{-1}$. Some wiggles are evident if one ignores the systematic uncertainties. The spectrum reveals a hardening at around 100 GeV and a steepening above ~ 400 GeV. More specifically, the spectrum can be fitted by a broken power-law with indices -3.070 ± 0.025 for $\mathcal{E} < 100$ GeV, -2.986 ± 0.031 for $100 < \mathcal{E} < 400$ GeV, and -3.266 ± 0.116 for $400 < \mathcal{E} < 1000$ GeV⁶⁸. So in general, all detectors reveal *an excess* beyond 100 GeV on the otherwise softening spectrum, although different instrumental teams do not agree on the detailed spectral shape.

The other independent indication of the presence of a possible deviation from the standard picture came from the recent measurements of the positron-to-electron ratio, between 1.5 and 100 GeV by the PAMELA satellite experiment. PAMELA found that the positron fraction changes slope at around 10 GeV and begins to increase steadily up to 100 GeV^{21,22}, confirming the tendency revealed in some earlier experiments with lower significance and in a narrower energy range (see Section 2.1). This rising behavior is very different from that predicted for the secondary positrons produced by collisions of CR nuclides and the ISM (see eq.(7))^{59,61}.

We summarize the data in Fig.1 and Fig.2. The latest observations call for an additional component of electrons and positrons which is clearly unaccounted for in the standard CR model. The lack of an anti-proton excess found by PAMELA⁵⁷ plays a key role in understanding the origin of the electron/positron excess.

3. Physics of e^\pm CRs: Propagation Models and Cosmic Sources

3.1. The e^\pm background and the propagation effect

Galactic cosmic-ray propagation is a decades-old problem in astrophysics. The charged particles propagate diffusively in the Galaxy due to scattering with the random magnetic field^{7,59,14}. Interactions with the interstellar medium (ISM) and

8 *Y. Z. Fan, B. Zhang & J. Chang*

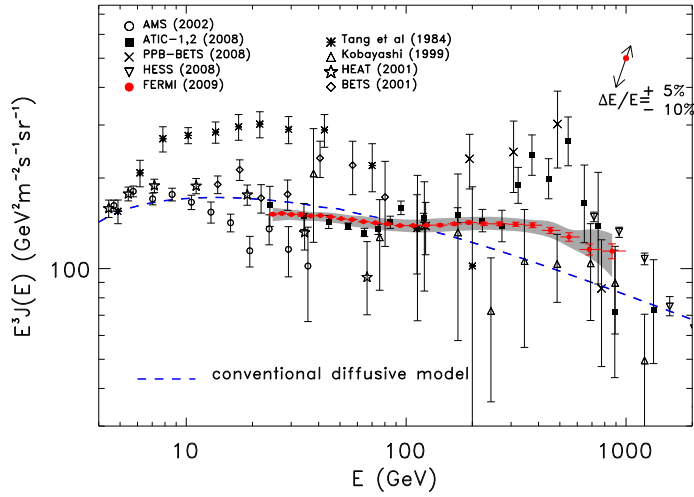


Fig. 1. Observational data against the background model estimates for the $e^+ + e^-$ energy spectrum (from Ref.26). J is the sum of the fluxes of electrons and positrons.

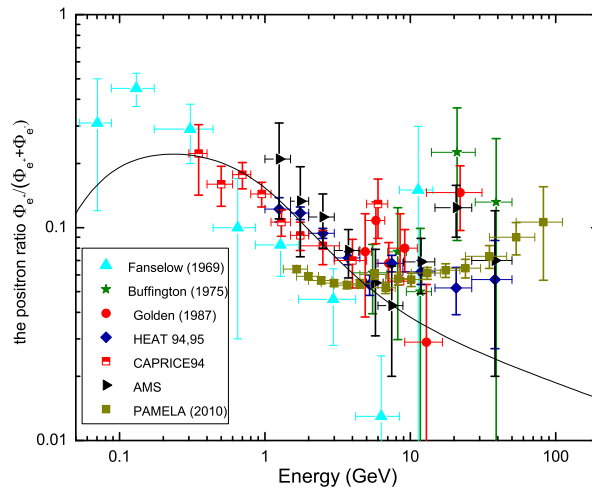


Fig. 2. Some measurements of the positron fraction up to an energy ~ 100 GeV. The data are from Refs. 32, 49, 20, 36, 37, 43, 22. The solid line is the positron fraction estimated by using eq.(7).

the interstellar radiation field would lead to energy losses of CRs. For heavy nuclei and unstable nuclei, there are also fragmentation processes by collisions with ISM and radioactive decays, respectively. The distribution of CRs is also modified by the convection driven by the galactic wind, and by the re-acceleration due to the interstellar shocks. As a result, the spectrum of the particles detected on Earth differs significantly from those emitted from the sources. The CR propagation equation for a particular particle species can be written in the general form^{59,14}

$$\begin{aligned} \frac{\partial \Psi(\vec{r}, p, t)}{\partial t} = & q(\vec{r}, p, t) + \vec{\nabla} \cdot (D_{xx} \vec{\nabla} \Psi - \vec{V} \Psi) + \frac{\partial}{\partial p} p^2 D_{pp} \frac{\partial \Psi}{\partial p} \\ & - \frac{\partial}{\partial p} [\dot{p} \Psi - \frac{p}{3} (\vec{\nabla} \cdot \vec{V}) \Psi] - \frac{1}{\tau_f} \Psi - \frac{1}{\tau_r} \Psi, \end{aligned} \quad (1)$$

where $\Psi(\vec{r}, p, t)$ is the CR density per unit total particle momentum p at the position r , which can be expressed as $\Psi(\vec{r}, p, t) dp = 4\pi p^2 f(\vec{p}) dp$ in terms of phase-space density $f(\vec{p})$; $q(\vec{r}, p, t)$ is the source term including primary, spallation, and decay contributions; D_{xx} is the spatial diffusion coefficient; \vec{V} is the convection velocity; D_{pp} is the momentum diffusion coefficient that describes diffusive reacceleration in terms of diffusion in the momentum space; \dot{p} is the momentum gain or loss rate; τ_f is the timescale for loss by fragmentation; and τ_r is the timescale for radioactive decay.

For primary particles such as protons and some heavy nuclei, the source function consists of two parts, the spatial distribution $f(\vec{r})$ and the energy spectrum $q(p)$. The former ($f(\vec{r})$) may follow the distribution of the possible sources of CRs, for example, the supernova remnants (SNRs). The injection spectrum $q(p)$ is usually assumed to be a power law (or a broken power law) function with respect to momentum p . The source function of the secondary particles, which depends on the distributions of primary CRs and the properties of the ISM, is given by^{59,61}

$$q(\vec{r}, p, t) = \beta c \Psi_p(\vec{r}, p, t) [\sigma_H(p) n_H(\vec{r}) + \sigma_{He} n_{He}(\vec{r})], \quad (2)$$

where βc is the velocity of the injecting CRs (c is the speed of light); $\Psi_p(\vec{r}, p, t)$ is the density per unit momentum p of the primary CRs; σ_H and σ_{He} are the cross sections of producing the secondary particles from the interactions between primaries and the H and He targets; n_H and n_{He} are the interstellar hydrogen and helium number densities, respectively. The secondary electrons/positrons are mainly produced in the proton – proton and proton – He collisions, resulting in charged pions and kaons, which further decay as $K^\pm \rightarrow \pi^\pm + \pi^0$, $K^\pm \rightarrow \mu^\pm + \nu_\mu$, $\pi^\pm \rightarrow \mu^\pm + \nu_\mu$ and $\mu^\pm \rightarrow e^\pm + \bar{\nu}_\mu + \nu_e$. The spatial diffusion coefficient is usually regarded as isotropic and is described by a function

$$D_{xx} = \beta D_0 (\rho / \rho_0)^\delta, \quad (3)$$

where ρ is the magnetic rigidity (defined as momentum p per unit charge).

In addition to spatial diffusion, scattering of CR particles on randomly moving MHD waves leads to stochastic acceleration, which is described in a transport

10 *Y. Z. Fan, B. Zhang & J. Chang*

equation as diffusion in momentum space with a diffusion coefficient D_{pp} , which is related with the spatial diffusion coefficient D_{xx} through⁶⁰

$$D_{pp}D_{xx} = \frac{4p^2v_A^2}{3\delta(4-\delta^2)(4-\delta)w}. \quad (4)$$

Here v_A is the Alfvén speed, and w (may be taken as 1) is the ratio of magnetohydrodynamic wave energy density to the magnetic field energy density, characterizing the level of turbulence^{60,61}.

The convection velocity \vec{V} , which is related to the galactic wind, is assumed to be cylindrically symmetric and increases linearly with height z from the galactic plane⁵⁹. Besides transporting particles, convection also causes adiabatic energy losses of CRs as the wind speed increases away from the disk¹⁴.

Practically most our knowledge of CR propagation is learned from studying secondary CRs. This is because the secondary production functions can be computed with reasonable precision from the locally observed primary spectra, cross sections, and interstellar gas densities. The propagation parameters are determined by comparing the predicted secondaries after the propagation effect with the observations. The typical parameters found in the CR modeling are $D_0 \sim (3-5) \times 10^{28} \text{cm}^2 \text{s}^{-1}$ and $\delta \sim 1/3$ for $\rho_0 \sim 1 \text{GV}^{14}$.

In some simplified cases the propagation equation (1) can be solved analytically using the Green function method^{62,63}. In most realistic cases an analytical solution is not available. A numerical model, widely known as the GALactic PROPagation (GALPROP; <http://galprop.stanford.edu>) model, was developed by Strong and Moskalenko to solve the problem^{59,14}. The main parameters for a given GALPROP model include the CR primary injection spectra, the spatial distribution of CR sources, the size of the propagation region, the spatial and momentum diffusion coefficients and their dependencies on particle rigidity. The ISM and interstellar radiation field are adopted to calculate fragmentations and energy losses of CRs. The parameters are tuned to reproduce the CR spectra observed on Earth. The publicly available GALPROP code can give relatively good descriptions of almost all kinds of CRs, including the secondaries such as anti-proton as well as diffuse γ rays^{59,14}.

As an example, for the Moskalenko & Strong's model 08-005 without reacceleration⁶⁴, the calculated primary electron and secondary electron and positron background fluxes can be parameterized as follows⁶³

$$\begin{aligned} \Phi_{e^-}^{\text{bg,prim}} &= \frac{0.16\varepsilon^{-1.1}}{1 + 11\varepsilon^{0.9} + 3.2\varepsilon^{2.15}} (\text{GeV}^{-1} \text{cm}^{-2} \text{s}^{-1} \text{sr}^{-1}), \\ \Phi_{e^-}^{\text{bg,sec}} &= \frac{0.7\varepsilon^{0.7}}{1 + 110\varepsilon^{1.5} + 580\varepsilon^{4.2}} (\text{GeV}^{-1} \text{cm}^{-2} \text{s}^{-1} \text{sr}^{-1}), \\ \Phi_{e^+}^{\text{bg,sec}} &= \frac{4.5\varepsilon^{0.7}}{1 + 650\varepsilon^{2.3} + 1500\varepsilon^{4.2}} (\text{GeV}^{-1} \text{cm}^{-2} \text{s}^{-1} \text{sr}^{-1}). \end{aligned} \quad (5)$$

In the above the energy ε is in units of GeV (i.e., $\varepsilon \equiv \mathcal{E}/1 \text{ GeV}$). For $\varepsilon \gg 1$, we

have

$$\Phi_e = \Phi_{e^-}^{\text{bg,prim}} + \Phi_{e^-}^{\text{bg,sec}} + \Phi_{e^+}^{\text{bg,sec}} \approx \Phi_{e^-}^{\text{bg,prim}} \propto \varepsilon^{-3.25}, \quad (6)$$

and

$$\mathcal{R}^{\text{bg}} = \Phi_{e^+}^{\text{bg,sec}} / (\Phi_{e^-}^{\text{bg,prim}} + \Phi_{e^+}^{\text{bg,sec}}) \approx 0.06\varepsilon^{-0.25}. \quad (7)$$

This set of background spectra agree well with the results of some more sophisticated numerical models⁶¹ derived for $\varepsilon > 10$.

The decreasing behavior of \mathcal{R}^{bg} can be understood more straightforwardly. In the diffusion models, the diffusion coefficient can be approximated as $D \propto \varepsilon^\delta$. The CRs are assumed to be produced with a power-law spectrum, $dN/d\varepsilon \propto \varepsilon^{-\alpha_{\text{cr}}}$. The observed spectrum is then a convolution of the source spectrum and propagation losses, giving $\Phi_{e^-}^{\text{bg,prim}} \propto \varepsilon^{-(\alpha_e + \delta)}$ for primary electrons, where α_e and α_p are the source power-law indices of CR electrons and protons, respectively. Positrons are secondary CRs formed from CR protons, and suffer additional propagation losses, implying $\Phi_{e^+}^{\text{bg,sec}} \propto \varepsilon^{-(\alpha_p + 2\delta)}$. Then approximately one has $\mathcal{R}^{\text{bg}} \propto E^{\alpha_e - \alpha_p - \delta}$ as long as $\Phi_{e^-}^{\text{bg,prim}} > \Phi_{e^+}^{\text{bg,sec}} + \Phi_{e^-}^{\text{bg,sec}}$. Usually one adopts $\alpha_e \approx \alpha_p$, so the standard model then predicts a CR positron-to-electron ratio that decreases with energy^{65,66,67}, in agreement with the tendency reported in eq.(7).

In the GALPROP code, there are several main approximations: a) The distribution of sources is continuous. b) All CRs are assumed to be from one single type of astrophysical sources, namely the supernova remnants (SNRs). c) The propagation of CRs is isotropic. Considering anisotropic propagation models can help to solve the problem of soft gradient in the radial dependence of the γ -ray flux, and can explain the large bulge-over-disk ratio in positron annihilation as observed by INTEGRAL. However, as shown in Fig.4 of Ref.71, the anisotropic propagation model gives a similar CR electron spectrum as the isotropic model in the energy range > 10 GeV. We therefore will not discuss the anisotropic propagation effect in the rest of the review. The change of the first two assumptions can give rise to interesting CR spectral signals, which we will come back to discuss later.

3.2. Sources of e^\pm cosmic rays

In general, there are five types of high energy electron/positron production processes:

- Acceleration of electrons in shocks or in magnetic turbulence. In strong shocks the highest electron energy is governed by the balance between energy gain (via shock acceleration) and loss (via synchrotron radiation in the magnetic field) and can be estimated as $\mathcal{E}_{e,\text{max}} \sim 20 \text{ TeV } \beta_{\text{sh}} \Gamma B_{\text{sh}}^{-1/2}$, where B_{sh} is the strength of the magnetic field in the shock region, β_{sh} is the velocity of the shock in units of speed of light c and Γ is the bulk Lorentz factor of the shock region.

- Cosmic rays accelerated at shocks produce secondary electrons/positrons inside the source through hadronic interactions. These interactions usually lead to production of charged pions or kaons, which decay to produce electrons and positrons. Besides the proton – proton and proton – He interactions discussed following eq.(3), some other processes include interactions between hadrons and photons, e.g. $\text{proton} + \gamma_{\text{bg}} \rightarrow \Delta^+ \rightarrow \text{neutron} + \pi^+ \rightarrow \text{neutron} + e^+ + \nu_e + \bar{\nu}_\mu + \nu_\mu$ (proton – γ process) and $\text{particle} + \gamma_{\text{bg}} \rightarrow \text{particle} + e^+ + e^-$, for which the energy thresholds are $\mathcal{E}_{\text{proton}}\mathcal{E}_{\gamma_{\text{bg}}} \approx (0.3 \text{ GeV})^2$ and $\mathcal{E}_{\text{particle}}\mathcal{E}_{\gamma_{\text{bg}}} \approx m_e m_{\text{particle}} c^4$, respectively.
- Annihilation of high energy photons with background photons, i.e., photon-photon pair production, $\gamma_{\text{high}} + \gamma_{\text{bg}} \rightarrow e^+ + e^-$. The energy threshold is $\mathcal{E}_{\gamma_{\text{high}}}\mathcal{E}_{\gamma_{\text{bg}}} \approx 2(m_e c^2)^2$ ⁶⁹.
- Pair production in ultra-strong magnetic fields, i.e., photon-magnetic field pair production, $\gamma + B \rightarrow e^+ + e^-$. The magnetic field B should satisfy $B \geq 6 \times 10^{13} \text{ G} (\mathcal{E}_\gamma/1 \text{ MeV})^{-1} \sin \vartheta^{-1}$, where ϑ is the angle between the photon and the magnetic field line⁷⁰. Such a strong magnetic field is expected in the vicinity of pulsars.
- Annihilation or decay of dark matter particles. Different from the above four processes, such kind of scenarios, although well motivated, are highly speculative and lack of solid experimental evidence.

3.3. Age and distance of the sources of e^\pm excess

The above five processes can take place in various astrophysical sources. However, it is difficult to pin down the exact source(s) of the observed e^\pm excess based on observations. This is because before reaching Earth the charged particles have been deflected by the interstellar magnetic fields. One can see this effect by estimating the Larmor radius $R_L \sim 10^{15} \text{ cm} (\mathcal{E}/1 \text{ TeV})(B_{\text{IG}}/3\mu\text{G})^{-1}$, which is much smaller than the distance of the CR sources to Earth, where $B_{\text{IG}} \sim 3\mu\text{G}$ is the strength of the interstellar magnetic field, and u_{cmb} . Nonetheless, one can reliably estimate the age and the distance of these sources in the following way. For an electron with energy \mathcal{E}_e , the total power of synchrotron and inverse Compton radiation in the Thomson regime is $P_r = \ell_0(\mathcal{E}/m_e c^2)^2$, where $\ell_0 \equiv 4\sigma_T c u_{\text{tot}}/3$. The characteristic cooling timescale can be estimated as $\sim \mathcal{E}/P_r$, i.e.,

$$\tau_{\text{rad}} \approx \frac{3m_e^2 c^3}{4\sigma_T u_{\text{tot}} \mathcal{E}} \approx 10^{15} \text{ s} \left(\frac{u_{\text{tot}}}{1 \text{ eV cm}^{-3}} \right)^{-1} \left(\frac{\mathcal{E}}{10 \text{ GeV}} \right)^{-1}, \quad (8)$$

where $u_{\text{tot}} = u_B + u_{\text{cmb}} + u_{\text{dust}} + u_{\text{star}}$, $u_B = B_{\text{IG}}^2/8\pi$ is the magnetic field energy density, u_{dust} and u_{star} are the photon energy densities of cosmological microwave background, dust emission, the star emission, respectively. The travel distance of

these CR electrons/positrons cannot exceed the characteristic CR diffusion radius

$$R_{\text{diff}} \sim 2\sqrt{D_0(\mathcal{E}/10 \text{ GeV})^\delta \cdot c\tau_{\text{rad}}} \\ \sim 4 \text{ kpc} \left(\frac{D_0}{10^{28} \text{ cm}^2 \text{ s}^{-1}}\right)^{\frac{1}{2}} \left(\frac{u_{\text{tot}}}{1 \text{ eV cm}^{-3}}\right)^{-\frac{1}{2}} \left(\frac{\mathcal{E}}{10 \text{ GeV}}\right)^{\frac{\delta-1}{2}}. \quad (9)$$

For $\delta \sim 1/3$, we find that for the observed electrons/positrons at $\sim 1 \text{ TeV}$, *the source should have an age $\leq \tau_{\text{rad}} \sim 10^{13} \text{ s}$ and should be within a distance $\leq R_{\text{diff}} \sim 1 \text{ kpc}$.* As a result, statistical fluctuations in the injection spectrum and spatial distribution of nearby sources within R_{diff} may cause significant deviations from the naive predictions in the conventional homogeneous and steady state scenario^{72,73,74}. Since R_{diff} is anti-correlated to \mathcal{E} , the deviations are more prominent at high energies.

In the following three sections, we will discuss three types of models that have been proposed to interpret the observed e^\pm excess, namely, the modified SNR models for the e^\pm background, new astrophysical sources, and dark matter.

4. Scenario I: Modified SNR Models for the e^\pm Background

Supernova remnants (SNRs) are the canonical sources of CRs⁷⁵. The kinetic energy of the SNRs is found to be comparable to that needed to accelerate Galactic CRs. The more direct evidence is the detection of the photons up to $\geq 10 \text{ TeV}$ from some SNRs, which are consistent with π^0 decay from hadronic interactions⁷⁶. SNRs have been traditionally regarded as the dominant source to contribute to the observed e^\pm background. This model can naturally account for a smooth, gradually softening e^\pm spectrum at high energies. The excess feature discussed above is not expected from the simplest model. In this section we discuss whether the excess is simply due to some factors that have been ignored in the conventional SNR models.

4.1. Inhomogeneity of SNRs?

As already mentioned, in the widely adopted code GALPROP the distribution of SNRs is assumed to be homogenous. Such an approximation would not affect the results of ion CRs significantly. For electrons, on the other hand, due to the significant cooling caused by magnetic fields and background photons, only the electrons generated within a distance $\sim 1 \text{ kpc}$ can reach Earth^{72,73} (see also Section 3.3). Within such a small volume, the SNR source distribution can be very inhomogeneous. Releasing the homogeneity assumption could therefore lead to significant modification of the detected e^\pm spectrum.

In the Milky Way, star formation is concentrated in spiral arms⁷⁷. The nearest spiral arm, the Sagittarius-Carina arm, is about 1 kpc away. The inhomogeneity effect of SR source distribution in such a distance scale is therefore very important to shape the observed electron/positron CR spectrum⁶⁶. Since R_{diff} is energy dependent (eq.(9)), an energy-dependent feature would appear. Low energy electrons ($\sim 1 \text{ GeV}$) can easily reach us from a larger radius where inhomogeneity is more

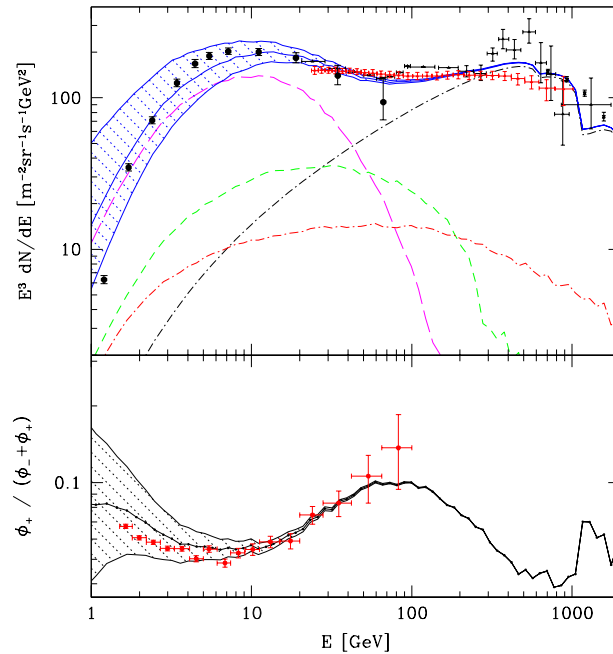


Fig. 3. Predictions of the inhomogeneous SNR models as compared with data (from Ref.66). *Top Panel:* The expected electron and positron spectra – Primary arm electrons (long dashed purple), primary disk electrons with nearby sources excluded (short dashed green), nearby SNRs (dot-dashed black), secondary positrons (dot-dashed red), and their sum (blue). The hatched region describes the solar modulation range (0.2-1.2 GeV). *Bottom Panel:* Model results and the measured PAMELA data for the positron fraction. The shaded region is variability expected from solar modulation effects (from Ref.66).

averaged out. On the other hand, electrons with higher energies (≥ 10 GeV) can arrive Earth only from very nearby sources since they would otherwise have cooled via synchrotron and inverse-Compton radiation before reaching Earth. These very nearby sources would present a bump in the e^\pm spectrum in the > 100 GeV range, as observed by ATIC and Fermi. Pairs formed in the local vicinity through the proton/ISM interactions can reach the solar system also at high energies. As shown in Fig.3, both the PAMELA-observed increase of the positron-to-electron ratio between 1 and 100 GeV and the ATIC-observed e^\pm excess around ~ 600 GeV can be attributed to the inhomogeneity of SNRs^{66,67}.

One interesting prediction of the inhomogeneous SNR model is that the positron-to-electron ratio should start to drop at energy $\mathcal{E} \sim 100$ GeV, just above the present PAMELA measurement (see Fig.3). It should reach a minimum around the “ATIC peak”, where it should start to rise again. This is because the nearby SNRs mostly contribute to primary electrons near the “ATIC peak”, without significantly increasing secondary positrons. Such a prediction is in stark contrast to the case where the

> 100 GeV excess is due to a primary source of pairs (e.g. either the pulsar model or the dark matter models), in which the positron fraction is expected to keep rising at a few hundreds GeV until reaching $\sim 50\%$. The positron fraction behavior above 100 GeV is the smoking gun to test this inhomogeneous SNR model (and the pair production models).

4.2. Acceleration of the secondary e^\pm in SNRs?

In the standard model, primary cosmic rays are accelerated in SNRs while the secondary e^\pm are not. In reality the secondary production also takes place in the same region where cosmic rays are being accelerated. These secondary e^\pm participate in the acceleration process and turn out to have a flatter spectrum relative to the primaries at high energies. This could be responsible, after propagation in the Galaxy, for the observed PAMELA anomaly^{79,80}. As found in solving the transport equation, the downstream equilibrium spectrum of secondary electrons produced in the acceleration region has two terms. One term traces the spectrum of the high energy primary CRs, i.e., $\propto \mathcal{E}^{-\kappa}$. The other term has a spectrum $\propto \mathcal{E}^{-\kappa+\delta}$, where the factor \mathcal{E}^δ arises from the momentum dependence of the diffusion coefficient^{79,80}. As long as the second term dominates, the spectrum gets flattened. This effect was noted earlier as a general expectation for the secondary-to-primary ratio in the presence of continuous Fermi acceleration^{81,82}. By simulating the spatial and temporal distributions of SNRs in the Galaxy according to their known distribution statistics, the $e^+ + e^-$ energy spectrum measured by Fermi LAT can be interpreted within such a secondary e^\pm acceleration model⁸⁰ (see Fig.4). A large portion of the model parameter space seems to lead to overprediction of TeV flux as compared with the H.E.S.S. Observations. Considering the large systematic uncertainties of H.E.S.S. and large uncertainties of the model parameters, the model can make a case to account for both the e^\pm excess and the positron fraction excess. Future high quality TeV data can give a more reliable test to this model.

The secondary particle acceleration model has several interesting predictions. In particular, all other secondary particles (including baryonic particles) are also accelerated. As a result, the antiproton to proton ratio should also increase with energy. This is a clean criterion to differentiate this model from some other astrophysical models for positron fraction excess (e.g. pulsar models). Some dark matter models however share the same prediction, and therefore cannot be differentiated based on this criterion. A similar effect applies to secondary nuclei such as titanium and boron⁸⁴. These predictions can be soon tested with the data from PAMELA and the forthcoming AMS-2 mission. Finally, since this model invokes strong hadronic interactions, one would naturally expect strong hadronic neutrino signals from nearby SNRs, so that IceCube has good prospects to detect them.

This model requires that secondary positrons can escape the shock region to reach Earth. For young SNRs, magnetic field amplification by the shock wave is very effective, so that synchrotron cooling of e^\pm is significant. High energy e^\pm may

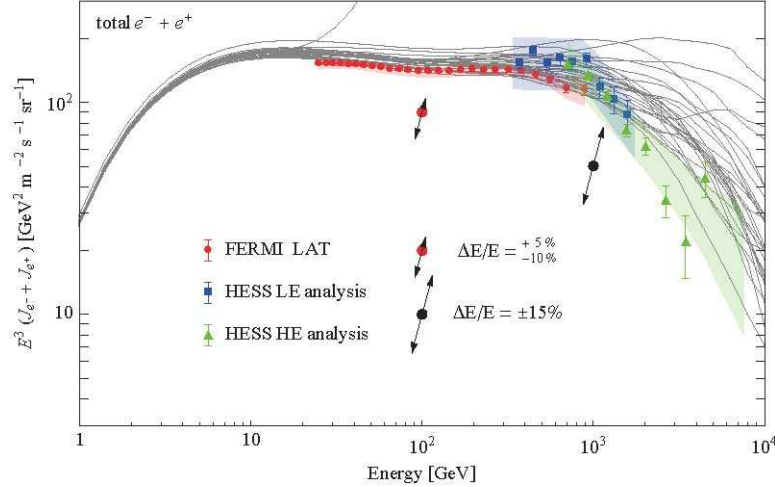


Fig. 4. The spectrum of the total cosmic ray electrons and positrons expected in the secondary particle acceleration model (The figure is from Ref.80).

not be able to escape from the acceleration site. As a result, the SNRs invoked in this model should be old enough.

4.3. e^\pm pair production in the photon-proton interaction in young SNRs?

Despite the cooling constraint discussed above, young SNRs have been argued to be an attractive candidate to solve the excess puzzle. In young SNRs, interactions of newly formed CR nuclei and background radiation may produce energetic e^\pm pairs, which would change the CR spectrum at the source. Considering a photon field at the source peaking in the optical/infrared band ($\mathcal{E}_{\gamma_{\text{bg}}} \sim \text{eV}$), pair production occurs at $\sim (m_e c^2 / \mathcal{E}_{\gamma_{\text{bg}}}) m_{\text{particle}} c^2$, which is ~ 1 PeV for protons and \sim a few PeV for helium⁸⁵. These correspond to the “knee” of the cosmic CR spectrum. In the rest frame of the CR nuclei, the secondary electrons/positrons have energies around MeV, which turn out to be about TeV in the observer’s frame. It is striking to note that this is just the energy range where the e^\pm excesses were observed by ATIC, Fermi, and H.E.S.S. Furthermore, the energy density of the excess electrons observed by ATIC is about $u_{e^\pm} \sim 3 \times 10^{-5} \text{ eV cm}^{-3}$ between 0.1 and 1 TeV, which is of the order of the energy density due to CR energy loss assuming a spectral break from 2.7 to 3.1 at energy ~ 1 PeV. These coincidences are the motivations of the photon-CR interaction model⁸⁶. Indeed the interaction between CR nuclei and background photons may naturally bridge the “knee” of the CR spectrum and the e^\pm excess, provided that the optical background photons have a thermal distribution with a temperature $T_{\text{opt}} \sim 5000 - 7000 \text{ K}$ ⁸⁶. Such a dense background photon field is possible in the vicinity of young SNRs.

One potential problem not addressed by Ref.86 is whether the resulting pairs can escape from the source. As discussed above, young SNRs tend to have strong magnetic fields. Together with the very dense background photons invoked to produce e^\pm , strong cooling of the produced secondary e^\pm is expected, which would lead to the production of strong infrared/optical synchrotron radiation and GeV-TeV inverse Compton radiation. One needs to check whether the escaped e^\pm can still reach the desired energy to account for the observed excess.

4.4. Klein-Nishina suppression of electron/positron cooling?

An electron or positron moving in a dense soft photon bath would lose energy via inverse Compton (IC) scattering⁸⁷ and produce a high-energy IC component at $\mathcal{E}_{\text{ic}} \approx \frac{2\gamma_e^2 \mathcal{E}_{\text{bg}}}{1+g}$, where $g \equiv \gamma_e \mathcal{E}_{\text{bg}}/m_e c^2$ and $\gamma_e \equiv \mathcal{E}/m_e c^2$ is the Lorentz factor of the electron. In the Thompson regime, $g \ll 1$, so $\mathcal{E}_{\text{ic}} \approx 2\gamma_e^2 \mathcal{E}_{\text{bg}}$. In the extreme Klein-Nishina regime, $g \gg 1$, one has $\mathcal{E}_{\text{ic}} \approx \gamma_e m_e c^2$. The scattering cross section in the Klein-Nishina regime is also greatly reduced, so that the electron/positron cooling rate drops correspondingly. The strength of the drop is proportional to the energy density of the seed photons. One may define the critical Klein-Nishina energy of electrons $\mathcal{E}_{\text{KN}} \sim 0.3m_e^2 c^4/\mathcal{E}_{\text{bg}}$, above which is the Klein-Nishina effect becomes significant⁸⁸. This corresponds to ~ 44 GeV for a typical B star and ~ 180 GeV for typical G-K stars. So given the galactic diffuse optical background from stars, the effect takes place in the energy range where electron/positron excess is observed to appear^{88,89}. Associated with the drop in energy loss rate in the Klein-Nishina regime is a gradual hardening of the cosmic ray e^\pm spectrum. The spectral structure in the FERMI and H.E.S.S. data may be reproduced in this way^{88,89} provided that: (1) The energy density of the seed photons is significantly higher than that of the magnetic field (so that IC cooling is more significant than synchrotron cooling); (2) the star-to-dust emission ratio $u_{\text{star}}/u_{\text{dust}}$ is large enough⁸⁹, so that the dominant IC cooling is with respect to star optical emission. This requirement is needed since IC off the dust emission in the far-infrared range is still in the Thomson regime even for relatively energetic electrons. Such a cooling effect would compete with the Klein-Nishina cooling effect if u_{dust} is not suppressed, which would smear the e^\pm spectral feature. This Klein-Nishina-related feature was not noticed previously in the GALPROP calculations⁵⁹ since a small $u_{\text{star}}/u_{\text{dust}}$ was adopted.

The Klein-Nishina effect affects both primary electrons and secondary positrons. Besides accounting for the excess in the total e^\pm spectrum, it can affect the positron-to-electron ratio and may be able to reproduce the PAMELA result⁸⁹. The u_{star} and the number density of the interstellar medium are however required to be about 100 times larger than the average values expected in the Galactic disk. Such extreme parameters may apply to the vicinities of young supernova remnants. A caveat is again high-energy e^\pm may not be able to overcome strong cooling and escape from such sources (see §4.3).

5. Scenario II: New Astrophysical Sources

In the previous section, it is assumed that SNRs are the sole source of cosmic ray electrons/positrons. Such an assumption may well be wrong since other astrophysical objects can also produce high energy electron/positron cosmic rays. As early as in 1970s, pulsars had been suggested as the source of the CR electrons/positrons⁹⁰. Some widely discussed objects include Vela and Geminga^{90,72,91,92}. Some other nearby cosmic ray accelerators, such as microquasars or an ancient gamma-ray burst, are also possible candidates. In this section we discuss these alternative astrophysical sources.

5.1. Pulsars

Pulsars are strongly magnetized, rapidly rotating neutron stars that are powered by spin down and emit broad-band pulsed electromagnetic radiation⁹³. They are important particle accelerators. Direct evidence comes from the recent Fermi discovery of nearly 50 high confidence gamma-ray pulsars with emission above 100 MeV^{94,95}. Three accelerator sites have been discussed in the literature. 1. Polar cap models invoke a charge-depleted gap near the magnetic polar cap region^{96,97,98} in which primary particles are accelerated and high energy γ -rays are radiated via curvature radiation of inverse Compton scattering. The high energy γ -rays interact with strong magnetic fields near the pole and produce electron-positron pairs. These secondary pairs cool via synchrotron radiation or resonant inverse Compton scattering and produce higher generation γ -rays and pairs, leading to a photon-pair cascade^{99,100}. 2. Outer gap models^{101,102,103} invoke a charge depleted gap developed beyond the “null” charge surface but enclosed by the last open field line. Particles are accelerated to high energies in the intense electric field parallel to the magnetic field lines inside the outer gap, and γ -rays are produced via inverse Compton scattering or curvature radiation. The γ -rays interact with other softer photons in the magnetosphere to produce e^\pm pairs. 3. Slot gap models^{104,105} invoke an elongated gap near the last open field line, the electric field inside which is immune from pair screening thanks to its favorable geometry. Particles can be accelerated from the surface all the way to the light cylinder. Almost the entire electric potential can be utilized for acceleration. Outer gaps cannot exist in old pulsars (e.g. $t > 10^7$ yr), while polar gaps and slot gaps can exist in all active pulsars. Recent Fermi observations disfavor the polar cap origin of most γ -rays, although both the outer gap and the slot gap models are still reasonable candidates for pulsar γ -ray emission, and hence, for energetic particle acceleration. Outside the magnetosphere, pairs can be re-accelerated in shocks as the pulsar wind interacts with the ambient medium. For young pulsar systems, a bright pulsar wind nebula would exist inside the supernova remnant, which radiate in a broad band from X-rays up to TeV energies.

To estimate the CR electron/positron production from pulsars, one needs to know the total energy budget of a pulsar and the fraction of this energy that is converted into pairs. For the first purpose we adopt the classical rotating magnetic

dipole model^{106,107,108}, in which the pulsar loses its rotational energy through magnetic dipole radiation. The spin-down power is estimated as

$$L_{\text{dip}} = I\Omega\dot{\Omega} \simeq 2.6 \times 10^{40} \text{ erg s}^{-1} B_{p,12}^2 R_{s,6}^6 \Omega_{0,3}^4 (1 + t/\tau_0)^{-2}, \quad (10)$$

where B_p is the polar cap dipolar magnetic field strength of the pulsar, R_s is the pulsar radius, Ω_0 is the initial angular frequency of rotation (the current angular frequency of the rotation is $\Omega = 2\pi/P = \Omega_0(1 + t/\tau_0)^{-1/2}$), $\tau_0 = 1.6 \times 10^{10} B_{p,12}^{-2} \Omega_{0,3}^{-2} I_{45} R_{s,6}^{-6}$ sec is the initial spin-down timescale of the pulsar, $I \sim 10^{45}$ g cm² is the typical moment of inertia of the pulsar¹⁰⁶. Here the convention $Q_x = Q/10^x$ has been adopted in cgs units. The polar cap dipolar magnetic field strength at the surface is $B_p = 6.4 \times 10^{19} \sqrt{P\dot{P}}$ Gauss. Following Refs.109, 110 we denote f_{e^\pm} as the fraction of the rotational energy that is deposited in the cosmic ray e^\pm pairs. The energy output rate of e^\pm pairs can be then estimated as $\dot{E}_{e^\pm, \text{out}} = f_{e^\pm} I\Omega\dot{\Omega}$. It is usually suggested that the mature pulsars (with ages $\sim 10^5$ years and without associated SNRs) rather than the young pulsars can contribute to the observed e^\pm pair flux because the produced pairs are no longer trapped and lose energy in the nebula. The total energy output of the e^\pm pairs for a mature pulsar can be estimated as

$$E_{e, \text{out}} = \frac{f_{e^\pm}}{1 + x_0} \frac{I\Omega_0^2}{2}, \quad (11)$$

where $x_0 \sim 10^5$ years/ τ_0 . The parameter f_{e^\pm} may be time-dependent and is not well determined. A quantitative discussion of plausible values was recently presented in Ref. 109 (Some more model-dependent estimates of the e^\pm pair production rate can be found in Refs.111, 112, 113). In the context of a standard model of pulsar wind nebulae, a reasonable range for f_{e^\pm} falls between 1% and 30%. For typical parameters $(I_{45}, \Omega_0, x_0) \sim (1, 300, 10)$, we have $E_{e, \text{out}} \sim 5 \times 10^{47} (f_{e^\pm}/0.1)$ ergs. To account for the observed ATIC electron/positron excess by a single pulsar, the pulsar needs to be within a radius $r \sim 0.4$ kpc $(E_{e, \text{out}}/5 \times 10^{47} \text{ erg})^{1/3} (u_{e^\pm}/3 \times 10^{-5} \text{ eV cm}^{-3})^{-1/3}$. Considering that only a fraction of electrons/positrons can reach an energy above 100 GeV, the source should be even closer. Indeed there are a few nearby intermediate age pulsars within 0.3 kpc (e.g. Geminga at 0.16 kpc, PSR 0656+14 at 0.29 kpc, and Vela at 0.29 kpc). For a complete pulsar catalog with distance information, see <http://www.atnf.csiro.au/research/pulsar/psrcat/>.

Once the total energy output is specified, the injected electron-positron spectrum is fully defined by its spectral shape. The pairs generated from various gaps usually are not energetic enough, and they usually do not form a simple power law spectrum. In order to be relevant to the CR e^\pm excess, one needs to assume that these pairs are re-accelerated in pulsar wind nebula shocks. It is well known that the e^\pm escaping pulsar wind cannot be accelerated to arbitrarily high energies. Depending on the pulsar environment, a cut-off is expected, usually in the energy range around TeV. The precise position of the cutoff $\gamma_{e^\pm, \text{max}}$ is rather uncertain,

20 *Y. Z. Fan, B. Zhang & J. Chang*

and it critically depends on the pulsar age and on the magnetic field strength in the pulsar wind nebula¹¹⁴.

The pulsar pair spectrum is usually assumed to take the form

$$\frac{dN_{e^\pm}}{d\gamma_{e^\pm}} \propto \gamma_{e^\pm}^{-\kappa} e^{-\gamma_{e^\pm}/\gamma_{e^\pm, \max}}. \quad (12)$$

For a point source with a power-law spectrum $\frac{dN_{e^\pm}}{d\gamma_{e^\pm}} \propto \gamma_{e^\pm}^{-\kappa}$, the energy distribution of the pairs reaching Earth can be conveniently handled as¹¹⁵

$$n(R, t, \gamma_{e^\pm}) = \frac{dN_{e^\pm}/d\gamma_{e^\pm} [r/R_{\text{diff}}(t, \gamma_{e^\pm})]^3 e^{-[r/R_{\text{diff}}(t, \gamma_{e^\pm})]^2}}{\pi^{3/2} r^3 (1 - \ell_0 t \gamma_{e^\pm})^{2-\alpha}}, \quad (13)$$

where the spectrum has a cut off at $\gamma_c = 1/(\ell_0 t)$. The energy loss rate and age then set a maximal energy of particles that reach Earth today, with a diffusion radius¹¹⁵

$$R_{\text{diff}}(t, \gamma_{e^\pm}) \approx 2\{\mathcal{D}(\gamma_{e^\pm})ct[1 - (1 - \gamma_{e^\pm}/\gamma_c)^{1-\delta}]/[(1 - \delta)\gamma_{e^\pm}/\gamma_c]\}^{1/2}, \quad (14)$$

where $\mathcal{D}(\gamma_{e^\pm}) \approx \mathcal{D}_0(1 + \gamma_{e^\pm}/\gamma_*)^\delta$ and $\gamma_* \approx 6 \times 10^3$.

Following the above procedure, several authors have calculated the contribution of one or more nearby pulsars to the observed e^\pm spectrum^{109,110,116}. By picking a few nearby known pulsars and employing some suggested energy output models, one is able to reproduce the spectral features and the intensities of the reported e^\pm excess, with reasonable values for the e^\pm output efficiency (see Fig.5 for illustration). The advantage of this model is the lack of an anti-proton excess, in agreement with the PAMELA observation⁵⁷. Since electrons and positrons are produced in pairs in the pulsar models, the positron fraction would achieve 50% at high energies in the pulsar model. Another prediction of the pulsar model for the e^\pm excess is that at higher energies, the electron/positron flux measured at Earth will be dominated by a few nearby pulsars, and therefore the spectrum would host wiggly-like features^{51,109,110}. The presence of such features at high energies would strongly suggest a pulsar origin of the anomalous contribution to the electron/positron fluxes. The hardening of the CR electron spectrum detected by H.E.S.S at an energy ~ 4 TeV, if confirmed in the future, may be taken as a support to the pulsar model, although the inhomogeneous distribution of SNRs may also produce the wiggly-like structure in the electron/positron spectrum at TeV energies. The differentiation could be made by evaluating the corresponding positron-to-electron ratio, which should be small for the SNR model (since secondary positrons are much rarer than primary electrons), but large for the pulsar models (electrons and positrons are produced in pairs).

5.2. Microquasars

Microquasars are a sub-group of accretion-powered X-ray binaries that process a relativistic jet. The companion can be either a high mass or a low mass star. The accretor itself is likely a rapidly spinning black hole, although a neutron star accretor is not ruled out. These objects display in miniature some of the properties of quasars,

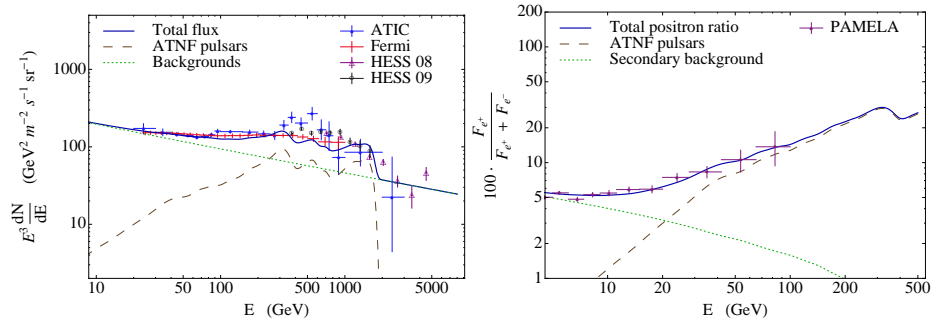


Fig. 5. The spectrum of cosmic ray electrons and positrons expected in the pulsar model (from Ref.109).

accreting supermassive black holes with much higher luminosities, and hence, carry the name of “microquasar”¹¹⁷.

Although their physical origin is still unclear¹¹⁸, microquasars can be important sources of high energy cosmic rays^{119,120}. Gamma-ray flares with energy above 100 MeV have been detected from microquasars LS I +61 303¹²¹ and Cygnus X-3¹²², suggesting that they are powerful lepton accelerators. TeV electrons/positrons may be accelerated in the internal or termination shocks. More pairs can be produced as TeV gamma-rays attenuate with the UV/optical photons from the companion star. The net energy output of microquasars in the Galaxy is uncertain. An optimistic estimate suggests that up to 5 – 10% of the total CR luminosity can be contributed by such kind of objects^{119,120}. If correct, the energy output of microquasars is high enough to account for the detected CR e^\pm excess, as noted in Refs.24, 21. However, there are not many known nearby microquasars¹²³. The closest candidate is Cen X-4 at ~ 1.2 kpc. There is no detailed calculation of this model in the literature.

5.3. Gamma ray Bursts

Gamma-ray bursts (GRBs) are brief, intense flashes of soft (0.01 – 1 MeV) γ -rays in the sky, which are related to collapses of some massive stars or mergers of two compact stellar objects (two neutron stars or a neutron star and a black hole)¹²⁵. They were serendipitously discovered by Vela-satellites in late 1960s¹²⁴, and now are routinely detected by gamma-ray detectors and followed up by various telescopes in broad band (from radio to TeV). The event rate of nearby high-luminosity GRBs (those typical GRBs detected at cosmological distances) is roughly¹²⁶ $0.5 - 1 \text{ Gpc}^{-3} \text{ yr}^{-1}$, which corresponds to about 0.025-0.05 GRB per Myr per galaxy¹²⁷. Counting for those GRBs that do not beam towards us (with large uncertainty in the beaming correction factor)¹²⁸ - which are relevant since off-beam GRBs can also contribute to the diffuse e^\pm background - the rate can be as high as 1 GRB per $10^5 - 10^6$ yr per galaxy. Nearby low-luminosity GRBs can have a higher observed event rate (by a factor of 200-500)^{129,130}. Even if their collimation angles

are typically wider, the collimation-corrected event rate could be still higher than that of high-luminosity GRBs. As a result, it is possible that an ancient GRB in the solar neighborhood has produced enough e^\pm in a not distant past, which diffuse to Earth, leading to the observed excess¹³¹. Such a model can interpret both the total e^\pm excess and the positron fraction excess. Furthermore, depending model parameters, both a sharp feature measured by ATIC and a smooth feature measured by Fermi can be reproduced¹³¹.

There are however two caveats related to this scenario. First, it is not clear whether our galaxy is suitable to host cosmological GRBs. Observations show that cosmological GRBs typically reside in host galaxies that are different from ours^{132,133}. Some authors argued that Milky Way is too metal rich for bright GRBs¹³⁴, while some recent observations indicate that at least some GRBs can reside in host galaxies with metallicity as high as 0.3 solar value¹³⁵. More data are needed to settle down the debate. Second, even if bright GRBs can occur in our galaxy, it is non-trivial to deposit nearly same amount of γ -ray energy to TeV e^\pm pairs that escape from the GRB. One may envisage several pair production mechanisms in a GRB: (i) A baryonic fireball may be pair-rich in the early stage. However, most pairs would have annihilated when the fireball reaches the γ -ray radiation radius. (ii) In the prompt γ -ray emission region, TeV photons would annihilate with hard X-ray photons to produce TeV pairs, but these secondary pairs would quickly cool and re-radiate in the MeV regime; (iii) Prompt MeV photons may annihilate with the soft gamma-rays back-scattered by the circum-burst medium to produce pairs. These pairs have much lower energies. They may be reaccelerated by the external shock, but the escaping fraction may not be high. (iv) TeV photons emitted by the GRB (likely from external shock since the compactness parameter is too high for internal prompt emission) may interact with the “background” UV/optical photons to produce TeV pairs. These pairs can most easily escape. The question is how to get “background” UV/optical photons. Prompt bright optical flash similar to that detected in the naked-eye burst GRB 080319B¹³⁷ was invoked in the model of Ref.131. Such bursts are very rare, so that the chance of having a nearby GRB capable of accounting for the observed e^\pm excess is further reduced.

6. Scenario III: New Physics

Although the electron/positron excess can be explained within the astrophysical scenarios, another widely discussed scenario is that the excess is the signature of dark matter. The dark matter models have strong astrophysically motivations, and can interpret the excess data under the assumption of some (extreme) parameter regimes. In this section, we critically review these models. We begin with a brief review of the observational evidence of dark matter, and some widely-discussed dark matter candidates (see also Refs. 138, 139, 140, 141, 142, 143, 144, 145, 146, 147, 148, 149 for extensive reviews on dark matter candidates). We then go through various dark matter models (both annihilation and decay models) proposed in the

literature to interpret the electron/positron excesses, and comment on the observational constraints to the parameter spaces of these models. For a detailed review on the annihilation models, see also Ref.27.

6.1. Observational evidence for dark matter

It was recognized as early as 1930s¹⁵⁰ that some matter in the Universe is invisible. The non-baryonic nature of dark matter was established since early 1970s¹⁵¹. In the following we summarize several compelling arguments for the existence of non-baryonic dark matter.

6.1.1. Galactic rotation curves

The most direct evidence for dark matter in the galactic scale comes from the observations of the rotation curves of spiral galaxies (i.e., the graph of circular velocities v_c of stars and gas as a function of their distance r from the galactic center), which are usually obtained by measuring Doppler shifts of the 21 cm emission line of hydrogen gas. The detected rotation curves usually exhibit a characteristic flat behavior at a distance that is beyond the edge of the visible disks (see Fig. 6 for illustration). This implies that the mass $M_<(r)$ enclosed within a radius r follows $M_<(r) \propto r$ for $r \gg r_{\text{disk}}$, suggesting the existence of an extended dark matter halo. Measuring stellar velocity dispersion in elliptical galaxies also leads to a similar conclusion.

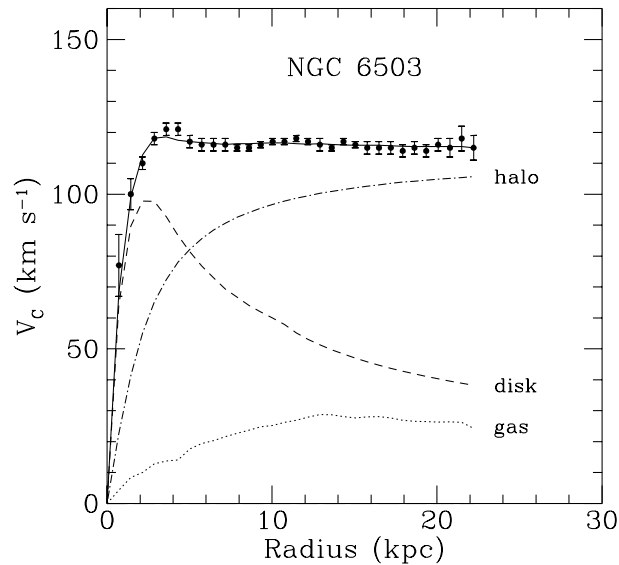


Fig. 6. Measured rotation curve of NGC6503 with best fit and the contributions from the dark matter halo, disk and gas (from Ref.153).

6.1.2. *Galaxy Clusters*

Galaxy clusters are the largest gravitationally bound objects in the Universe. Three independent methods all suggest that dark matter is the main mass that bind clusters together.

First, Newton's gravity law suggests that the velocity dispersion of galaxies is approximately $v^2(r) \sim GM_{<}(r)/r$. One can infer the total mass $M_{<}(r)$ from the measurements of the velocity dispersion and the size of a cluster (which can be determined if the redshift and angular size of the cluster are measured). In 1933, Zwicky¹⁵⁰ used this method to measure the mass-to-light ratio of the Coma cluster to be 400 times of the solar value. This gave the first hints of dark matter in the modern sense. The conclusion is confirmed by many follow-up measurements.

Second, according to the virial theorem, the gas temperature of the clusters may be estimated as $k_B T \approx 1.5 \text{ keV } (M_{<}(r)/10^{14} M_\odot)(1 \text{ Mpc}/r)$, where $M_{<}(r)$ is normalized to the baryonic mass derived from the star light $M_b \sim 10^{14} M_\odot$. However, the detected temperature is as high as $\sim 10 \text{ keV}$, suggesting the existence of much more massive dark matter, i.e., $M_{<}(r) \sim 6M_b$.

Finally, mass can be measured via the gravitational lensing effect predicted by Einstein's general theory of relativity¹⁵⁴. The mass of a lensing cluster can be inferred by the deflection angle $\theta \approx (GM_{\text{cl}}/dc^2)^{1/2}$ and the impact parameter d , both can be measured or inferred if the redshift of the lensing cluster is known. Usually the derived M_{cl} is much larger than the observed baryonic mass M_b , again indicating the existence of the large amount of invisible matter.

The most strong support to the dark matter picture came recently from an X-ray observation of the bullet cluster (Fig.7). The X-ray image (red) shows the distribution of baryonic mass (in the form of hot gas). The bulk of mass distribution as inferred by the gravitational lensing technique is denoted in blue, which does not trace the distribution of hot gas. Such a configuration is difficult to interpret within other competing models (e.g. the modified Newtonian dynamics), and strongly supports the dark matter interpretation.

6.1.3. *Cosmological constraints on energy densities*

Advances in technology have usher in the new age of precision cosmology. Wilkinson Microwave Anisotropy Probe (WMAP) can precisely measure the primordial fluctuation in the temperature map of the cosmic microwave background (CMB). By precisely locating the first acoustic peak in the power density fluctuation, WMAP clearly measured the curvature of the universe¹⁵⁶. Together with the observational results of Type Ia supernova that suggest an accelerating universe¹⁵⁷, very precise values of the parameters of the flat Λ CDM have been obtained. According to the latest 7-year WMAP data¹⁵⁸, the energy densities of various components of the Λ CDM model are $\Omega_b = 0.0456 \pm 0.0016$, $\Omega_{\text{dm}} = 0.227 \pm 0.014$, and $\Omega_\Lambda = 0.728 \pm 0.015$. An independent constraint on $\Omega_m = \Omega_{\text{dm}} + \Omega_b$ from the baryon acoustic peak is consistent with the WMAP result¹⁵⁹. All these strongly suggest that the universe

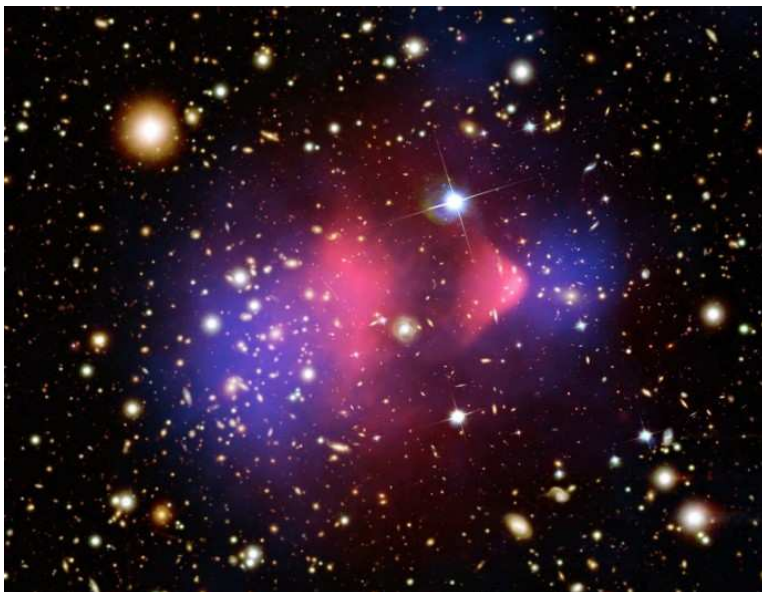


Fig. 7. The X-ray image by Chandra X-ray Observatory of the bullet cluster (red) over-imposed on the mass distribution (blue) derived from gravitational lensing. It is clearly shown that most of the mass does not trace the gas emission in the X-ray band. This Figure is from <http://www.spaceimages.com/hubucl1e06ph.html>.

is dark-matter dominated, and that the bulk of dark matter is not of the baryonic origin. An independent constraint on the amount of baryonic contribution to dark matter was derived from the MAssive Compact Halo Objects (MACHO) experiment, which showed that the micro-lensing detected MACHOs can only account for a small fraction ($\sim 20\%$) of the missing mass in the Milky Way and LMC halos¹⁶⁰.

6.2. Dark matter properties and possible candidates

The evidence for dark matter is compelling in all astrophysical scales. To be a viable dark matter candidate, one needs to satisfy some general requirements¹⁴⁶: (1) Dark matter must be *dark*, in the sense that it must have no (or extremely weak) interactions with photons. This is effectively saying that the electric charge of dark matter particles must be extremely smaller than the electron charge. (2) Self-interactions of the dark matter should be rather weak. This is manifested in the dark matter map of the Bullet Cluster (Fig.7). The collision between two galaxy clusters cause strong shocks of baryonic gas between the two clusters, while the two dark matter halos streamed through each other without noticeable interaction. (3) Interactions between dark matter and baryons must be very weak. Otherwise baryons and dark matter would fall together in the overdense region and form a baryon-DM disk in galaxies rather than forming an extended DM halo. (4) Dark matter cannot be mainly made up of standard model particles, since most leptons

and baryons are charged. The only potential candidate is neutrinos, but they are too “hot” and too light to be trapped in DM halos.

Physicists are never short of ideas of inventing non-baryonic dark matter candidates^{147,149}. Almost all current models of dark matter use the standard concept of quantum field theory to describe the properties of elementary particle candidates (for exceptions, see for instance Refs.161, 162). This means that the dark matter particles can be characterized by their mass and spin. In the following we summarize the properties of several widely discussed dark matter candidates. As shown in Table 1, the mass of the proposed candidates spans a wide range.

The most studied dark matter candidates are weakly-interacting massive particles (WIMPs). The main motivation for introducing WIMPs is the gauge hierarchy problem, namely, the observational constraint of the mass of the spin 0 Higgs Boson (a hypothetical massive particle in the Standard Model (SM) in particle physics), i.e. $114.4 \text{ GeV} < m_{\text{Higgs}} < 186 \text{ GeV}$ ^{163,164}, is much lighter than the Planck mass $M_{\text{Pl}} = 1.2 \times 10^{19} \text{ GeV}$. This suggests that SM is not the complete model, and there should be new physics in the energy range of the weak interaction scale $m_{\text{weak}} \sim 10 \text{ GeV} - \text{TeV}$. WIMPs are the predicted particles of the new physics, which naturally carries a mass with the similar energy scale. Very interestingly, this energy scale is broadly consistent with the energy scale of the PAMELA/ATIC/HESS/Fermi e^\pm excess. This was the main reason that the e^\pm excess stimulated the great excitement from the particle physics community. Three types of WIMPs, i.e. neutralinos and other supersymmetric particles, Kaluza-Klein particles in universal extra dimensions, and inert Higgs doublets, are discussed below. Some candidates, such as axions and sterile neutrinos, have too low an energy to be relevant to the e^\pm excess data. Since they are physically well motivated, we nonetheless include them for the sake of completeness.

Table 1. Properties of some Dark Matter Candidates (adapted from Refs.147, 149).

Type	Particle Spin	Approximate Mass Scale
Neutralino	1/2	10 GeV - 10 TeV
Kaluza-Klein UED	1	TeV
Inert Higgs Doublet	0	$\sim 50 \text{ GeV}$ or $\sim 650 \text{ GeV}$
Axion	0	$\mu\text{eV} - \text{meV}$
Sterile Neutrino	1/2	keV

6.2.1. *Neutralinos and other supersymmetric particles*

The most widely discussed WIMPs are neutralinos, one type of the supersymmetric (SUSY) particles. Supersymmetry (SUSY) is an ingredient in many superstring theories trying to unite all the fundamental forces of nature, including gravity¹⁶⁵. The gauge hierarchy problem is most elegantly solved by SUSY. In SUSY extensions of

the standard model, every standard model particle has a new, as yet undiscovered partner particle, which has the same quantum numbers and gauge interactions, but differs in spin by $1/2$. From the standpoint of dark matter, the lightest supersymmetric particle is naturally stable in models that conserve R -parity, which is defined as

$$R = (-1)^{3\mathcal{B}+L+2S}, \quad (15)$$

where \mathcal{B} is the baryon number, L the lepton number and S the spin of the particle^{138,141,147}. The ordinary particles and their superpartners have $R = +1$ and -1 respectively, which means that supersymmetric particles can only be created or annihilated in pairs in reactions of ordinary particles, or a single supersymmetric particle can only decay into final states containing an odd number of supersymmetric particles (plus some Standard Model particles). The idea that supersymmetric particles could be good dark matter candidates became attractive when it was realized that breaking of SUSY could be related to the electroweak scale, and that the supersymmetric partner of the photon (the photino) would couple to fermions with electroweak strength¹⁶⁶. Below we list some supersymmetric dark matter candidates^{167,141} with brief discussion.

- *Neutralinos* in models of R -parity conserving supersymmetry are by far the most widely studied dark matter candidates. Since the superpartners of the Z boson (zino), the photon (photino) and the neutral higgs (higgsino) have the same quantum numbers, they can mix to form four eigenstates of the mass operator called “neutralinos”¹⁶⁸. In many models the lightest of the four neutralinos χ turns out to be the lightest supersymmetric particle (LSP), which is, therefore, stable and can only be destroyed via pair annihilation (Neutralinos have spin $1/2$ and are their own antiparticles; that is, they are Majorana fermions). χ can be produced thermally in the hot early universe and leave approximately the right relic abundance to account for the observed $\Omega_{\text{dm}} h^2 \sim 0.1$, where $h \sim 0.71$ is the Hubble’s constant in units of $100 \text{ km s}^{-1} \text{ Mpc}^{-1}$. These facts make χ with a mass of roughly 10-10000 GeV, an excellent cold dark matter candidate. They may be detected directly through scattering in detectors, or indirectly through the decay products that result when neutralinos annihilate in pairs^{138,141}.
- *Sneutrinos* are the superpartners of the Standard Model neutrinos in the supersymmetric models. They have a spin 0, and have long been considered as dark matter candidates¹⁶⁷. If their mass is in the range of 0.55 – 2.3 TeV, the sneutrinos can have a cosmologically interesting relic density¹⁶⁹. From the direct detection searches sneutrinos have been excluded as the major component of the dark matter¹⁶⁹. However, in the supersymmetric models with the inclusion of right-handed fields, sneutrinos are still compatible with the current direct detection sensitivities and could be a viable dark matter candidate¹⁷⁰.

- *Gravitinos* are the spin $3/2$ superpartners of gravitons in the supersymmetric models, and could be the lightest, stable supersymmetric particle. Although strongly theoretically motivated, gravitinos as dark matter would be very difficult to observe due to their extremely weak interactions with ordinary matter¹⁷¹. Long lived gravitinos may impose problems to cosmology. For example, their presence may destroy the abundances of primordial light elements^{172,141}. These problems can be circumvented in some scenarios^{173,144}. For instance, in the case of a broken R-parity, the constraints from primordial nucleosynthesis are naturally satisfied and decaying gravitinos would lead to characteristic signatures in high energy cosmic rays¹⁷⁴.

6.2.2. *Kaluza-Klein Particles in Universal Extra Dimensions*

Our world appears to consist of $3 + 1$ dimensions (three spatial dimension and one time dimension). It is however possible that there exist other $\bar{\delta}$ spatial dimensions, which appear at much higher energy scales, as suggested by Kaluza and Klein in the 1920s. In the extra-dimension models, the $(3 + 1)$ -dimension space-time one experiences is a structure called a “brane”, which is embedded in a $(3 + \bar{\delta} + 1)$ space-time called the “bulk”. Upon compactification of the extra dimensions, all the fields propagating in the bulk have their momenta quantized in units of $p^2 \sim 1/\mathfrak{R}^2$, where \mathfrak{R} denotes the size of the extra dimensions¹⁴¹. As a result, for each bulk field a set of Kaluza-Klein (KK) states (i.e. Fourier expanded modes) appear. In the $3+1$ dimensional world, these KK states appear as a series of states with masses $m_n = n/\mathfrak{R}$, where n labels the mode number. Each of these new states contains the same quantum numbers, such as charge, color, etc¹⁴¹. Usually the standard model fields are assumed to be confined on the brane and only gravity is allowed to propagate in the bulk. However it might be possible for all the standard model particles freely propagate in the extra dimensions²⁰⁰. Such a scenario is the so-called universal extra dimensions. The simplest universal extra dimension models preserve a discrete parity known as the KK-parity, implying that the lightest KK particle (LKP) is stable and can be an interesting, possible dark matter candidate^{141,142}. The LKP is typically the level 1 partner of the hypercharge gauge bosons, denoted as $B^{(1)}$ ²⁰⁰. The WMAP limit of $\Omega_{\text{dm}} h^2 = 0.1131 \pm 0.0034$ ¹⁵⁸ corresponds to a mass of the dark matter candidate $B^{(1)}$ between roughly 0.5 to 1 TeV, depending on the exact form of the mass spectrum and the resulting co-annihilation channels^{201,147}. Current collider measurements give a constraint of $\mathfrak{R}^{-1} \geq 0.3$ TeV, whereas LHC may probe the KK mass parameter space up to $\mathfrak{R}^{-1} \sim 1.5$ TeV¹⁴².

6.2.3. *Inert Higgs*

Inert Higgs are a type of WIMPs that are introduced in one of the most minimal extensions of the standard model. Back in 1978, it was noted that a model with two

Higgs doublets containing a discrete symmetry could contain a state, the lightest neutral scalar or pseudoscalar boson, which is stable^{177,178}. It is the subject of the renewed interest recently since it could be used to solve the naturalness problem in the standard model¹⁷⁹. The possibility of one of the lighter neutral states in the enlarged Higgs sector to be the dark matter was also pointed out, and soon the basic properties of this “inert” Higgs candidate for dark matter were investigated¹⁸⁰. It turns out that this model contains a dark matter candidate, an “inert” particle that couples gauge bosons only and is stable due to its discrete symmetry. Taking into account the relic density constraints from WMAP and various theoretical and experimental constraints, the latest constraint on the mass of the Inert Higgs is $\sim 30 - 80$ GeV (middle mass range) or $\sim 500 - 800$ GeV (high mass range)¹⁸¹. Candidates in the middle mass range may annihilate through Z or through Higgs. Some solutions in the middle mass range may also have a large annihilation cross section, through loop corrections, into a pair of gamma rays. This is relevant for indirect detections of dark matter through annihilation at the Galactic Center, and such a gamma ray line would be easily observed by the Fermi satellite¹⁸². For the inert Higgs dark matter candidates in the high mass range, annihilation into W^\pm pairs is allowed with a large cross section¹⁸⁰.

6.2.4. Axions

Axions were introduced in an attempt to solve the strong CP problem in particle physics¹⁷⁵. They are still one of the leading dark-matter candidates. The axion mass is defined by

$$m_a = \frac{\sqrt{m_u m_d}}{m_u + m_d} m_\pi f_\pi \frac{1}{f_a} \approx 0.62 \text{ eV} \left(\frac{10^7 \text{ GeV}}{f_a} \right), \quad (16)$$

where $m_u \simeq 4$ MeV, $m_d \simeq 8$ MeV and $m_\pi \simeq 135$ MeV are masses of the up quark, down quark and pion, and $f_\pi \simeq 93$ MeV is the pion decay constant. The axion phenomenology is therefore determined by, up to a numerical factor, by one number only, i.e. the energy scale f_a of symmetry breaking. A variety of astrophysical observations and laboratory experiments constrain f_a to be between 10^9 GeV and 10^{12} GeV, suggesting an axion mass $m_a \sim 10^{-5} - 10^{-2}$ eV. Smaller masses would lead to an unacceptably large cosmological abundance, while larger masses are ruled out by combining of constraints from supernova 1987A, globular clusters, laboratory experiments, and the search for two-photon decays of relic axions^{176,147}. The lifetime of axion is $\tau(\text{axion} \rightarrow \gamma\gamma) \approx \frac{9 \times 10^{23} \text{ s}}{g_\gamma^2} \left(\frac{1 \text{ eV}}{m_a} \right)^5$, where g_γ is a model-dependent parameter and g_γ^2 is expected not to deviate from 1 significantly. In general, its very small mass makes axion not possible to interpret the 100 GeV e^\pm excess discussed in this review.

Within the SUSY theories, axions have spin 1/2 superpartners, which are called axinos. Models combining SUSY and the Peccei-Quinn¹⁷⁵ solution to the strong CP problem necessarily contain this particle. Depending on the model and the

SUSY breaking scheme, the axino mass can range from eV to GeV. Although widely believed to be only capable of acting as a warm, or hot dark matter candidate^{183,184}, it was recently shown that for quite low reheating temperatures, cold axino dark matter may be possible^{185,186}. Interesting astrophysical signals are expected from axinos if the R-parity is broken¹⁸⁷.

6.2.5. *Sterile Neutrinos*

The Standard (active) neutrinos were considered as a favored particle dark matter candidate in late 1970's, when the calculations of the massive neutrino relic density were first carried out^{188,189,190,191}. To account for the dark matter of a dwarf galaxy of velocity dispersion σ_d typically of order 100 km s^{-1} and core radius r_c typically 1 kpc, the neutrinos have to be “massive”^{193,146}

$$m_\nu \geq 120 \text{ eV} \left(\frac{100 \text{ km/s}}{\sigma_d} \right)^{\frac{1}{4}} \left(\frac{1 \text{ kpc}}{r_c} \right), \quad (17)$$

which is much larger than the upper limit $m_\nu < 2.3 \text{ eV}$ derived from the various experimental results (e.g. the tritium β -decay experiments at Mainz¹⁹²). Therefore the standard neutrinos are too light to be the dominant component of dark matter, although among the proposed candidates for non-baryonic dark matter standard neutrinos have the “undisputed virtue of being known to exist”¹³⁹.

Sterile neutrinos, unlike standard (active) neutrinos, do not interact through standard weak interactions^{194,195}. Instead, they communicate with the rest of the neutrino sector through fermion mixing^{196,197}. The existence of sterile neutrinos (right-handed or gauge singlet) is one of the most attractive explanations of the observed flavor oscillations of active neutrinos. Sterile neutrinos were proposed as dark matter candidates in 1994¹⁹⁴. Stringent cosmological and astrophysical constraints on sterile neutrinos come from the analysis of their cosmological abundance and the study of their decay products¹⁹⁸. A very recent analysis finds out that sterile neutrino DM with mass $\geq 2 \text{ keV}$ is consistent with all existing constraints¹⁹⁹. On the other hand, this mass is too low to account for the 100 GeV e^\pm excess feature discussed in this review.

6.3. *Dark matter models for the e^\pm excess*

In many dark matter models, the dark matter particles are their own anti-particles (Majorana fermions), and can annihilate with each other. There are several possible DM annihilation scenarios: (i) DM particles annihilate to standard model particle pairs, such as gauge bosons, quarks, and lepton pairs^{138,141,202,203,204,205}; (ii) DM particles annihilate via virtual internal bremsstrahlung processes to produce $e^+e^-\gamma$ ²⁰⁶; (iii) DM particles annihilate to new mediating particle pairs, which then decay to e^+e^- and other standard model particles^{207,208,209}. According to these scenarios, dark matter annihilation would lead to electron/positron pairs, and may account for the PAMELA/ATIC/HESS/Fermi e^\pm excess (see e.g., Refs.210, 211,

212, 138, 213, 141, 27, 207, 214, 215, 216, 217, 218, 206, 219, 220, 221, 222, 223, 224, 225, 226, 227, 228, 229, 230, 231, 232, 233, 234, 235, 236, 237, 238, 239, 240, 241, 242, 243, 204, 244, 245, 246, 247, 248, 209, 249, 250, 251, 252, 253, 254, 255, 256, 257, 258, 259, 260, 261, 262, 263, 264, 265, 266, 267, 268, 269, 270, 271, 272, 273, 274, 275, 276, 277, 278, 279). According to these scenarios, the resulting lepton spectra would have a cut off energy at the DM mass m_{dm} . Hence, the cutoff energy seen in Fermi/HESS (or ATIC) data would suggest $m_{\text{dm}} \sim 1.5$ (or 0.6) TeV.

The dark matter self-annihilation scenarios, which have been extensively discussed since 1970s, are not the only possibilities to produce signatures for dark matter indirect detections. Strictly speaking, the viability of a particle as a dark matter candidate does not require its absolute stability, but merely require that the dark matter lifetime τ_{dec} is much longer than the age of the Universe (i.e., $\tau_{\text{dec}} \gg 10^{18}$ s). Hence, if dark matter decays at a sufficiently high rate, the decay products might be detectable. In particular, if the DM decays predominately into leptons in a time scale $\tau_{\text{dec}} \sim 10^{26}$ s (which is long enough not to cause other cosmological problems), the detected 100 GeV e^{\pm} excess may be also reproduced (see e.g., Refs.173, 280, 61, 281, 282, 283, 284, 285, 286, 287, 288, 289, 290, 291, 292, 293, 294, 295, 296, 297, 298, 299, 300, 301, 302, 303, 304, 305, 306, 307, 308, 309, 310, 311, 312, 313, 314, 315). In these DM decay scenarios, the resulting e^{\pm} spectra would have a cutoff at an energy $\sim m_{\text{dm}}/2$. Hence, the cutoff energy seen in Fermi/HESS (or ATIC) data would suggest $m_{\text{dm}} \sim 3$ (or 1.2) TeV.

In both the annihilation and decay scenarios, the DM required in the modeling belongs to the WIMP category. This is encouraging since weak-scale particles make an excellent dark matter candidate, having the merit of the so-called WIMP miracle: In the simplest type of models of thermally produced dark matter, an average of the annihilation rate at the time of chemical decoupling can be estimated as $\langle \sigma v \rangle \approx 3 \times 10^{-26} (0.1/\Omega_{\text{dm}} h^2) \text{ cm}^3 \text{ s}^{-1}$, where $\langle \sigma v \rangle$ is the thermal average of the total annihilation cross section σ multiplied by velocity v . Taking the relative velocity of colliding DM particles at the decoupling time $v \sim 10^{10} \text{ cm s}^{-1}$, one has $\sigma \sim 10^{-8} \text{ GeV}^{-2} \sim \alpha^2/m_{\text{dm}}^2$, or $m_{\text{dm}} \sim 100[\alpha/(1/137)] \text{ GeV}$. This mass is in the energy range of weak interaction energy scale, and hence the particle is likely a WIMP.

In the following, we review the annihilation and decay models in turn.

6.3.1. Dark matter annihilation models

In the dark matter annihilation scenarios, the source term of the electrons/positrons is given by

$$q(\vec{r}, p) = \frac{1}{2} \left(\frac{\rho_{\text{dm}}(\vec{r})}{m_{\text{dm}}} \right)^2 \langle \sigma v \rangle \frac{dN_{e^{\pm}}}{d\mathcal{E}}, \quad (18)$$

where $\frac{dN_{e^{\pm}}}{d\mathcal{E}}$ is the energy spectrum of the electrons/positrons produced by DM annihilation, $\rho_{\text{dm}}(\vec{r})$ is the dark matter density distribution in the annihilating region,

and $\langle \sigma v \rangle \sim 3 \times 10^{-26} \text{ cm}^3 \text{ s}^{-1}$ based on the WIMPs miracle argument discussed above (i.e. the usual DM annihilation rate producing the e^\pm excess signal is also related to the annihilation rate producing the cosmological relic DM density). With a given $q(\vec{r}, p)$, one can solve the propagation equation (i.e., Eq.[1]) and get the final electron/positron spectra detected on Earth. For such a purpose, the density distribution of the dark matter halo is needed. Various models of DM halo density distribution have been proposed. Some popular ones can be parameterized as

$$\rho_{\text{dm}}(\vec{r}) = \rho_{\text{dm},\odot} \left(\frac{r_\odot}{r} \right)^\Upsilon \left[\frac{1 + (r_\odot/r_s)^\omega}{1 + (r/r_s)^\omega} \right]^{(\zeta - \Upsilon)/\omega}, \quad (19)$$

where $\rho_{\text{dm},\odot} \sim 0.3 \text{ GeV cm}^{-3}$ is the DM density in the vicinity of the sun, $r_\odot \sim 8.5 \text{ kpc}$ is the solar distance from the Galactic center, and the profile parameters $(\omega, \zeta, \Upsilon, r_s)$ are $(2, 2, 0, 5 \text{ kpc})$, $(1, 3, 1, 20 \text{ kpc})$, $(1, 3, 1.5, 30 \text{ kpc})$ for the Core Isothermal model³¹⁶, the Navarro, Frenk and White (NFW) model³¹⁷ and the Moore model³¹⁸, respectively. It is well known that only the TeV CR e^\pm produced within a distance $\sim 1 \text{ kpc}$ can reach us, i.e., $r \ll r_\odot$, hence the above 3 popular (but different) dark matter density distribution models give rise to rather similar CR e^\pm signals. The photon signals from these three different models, such as the GeV-TeV gamma-rays generated from inverse Compton scattering off the CMB photons by the TeV e^\pm 's or the synchrotron radiation of the TeV e^\pm 's, can however reach us from a much larger distance range including the core of the DM halo. These signals therefore can be very different for different models. If DM annihilation also produces hadronic pairs, the spectrum of the antiproton CRs can be also very different for different models, since antiprotons are more rigid and much less radiative so that they can reach from much larger distances. The non-detections of a prominent electromagnetic spectral signals in the radio (synchrotron origin) and GeV-TeV (inverse Compton origin) bands, as well as the non-detection of a prominent antiproton cosmic ray signal, therefore impose stringent constraints on the DM density profile and/or the DM annihilation properties.

Since the first release of the PAMELA data, many candidate WIMP DM models have been studied. The spectral shape of the observed e^\pm excess is not difficult to reproduce if the annihilations proceed mostly to leptons rather than to quarks, gauge bosons, and so on. For example, two-body annihilations directly into e^\pm pairs produce a hard spectrum, which can be adjusted to be consistent with the ATIC data. If the two-body final states are μ^\pm or τ^\pm pairs, their subsequent decays into e^\pm can produce a soft enough spectrum consistent with the Fermi and HESS data.

However, in all these models, the thermal average cross section multiplied by velocity $\langle \sigma v \rangle = 3 \times 10^{-26} \text{ cm}^3 \text{ s}^{-1}$ is found to be too small to account for the flux level detected by PAMELA/ATIC/Fermi/HESS. An unnaturally large “enhancement/boost factor”, $E_F \sim 10^2 - 10^3$, is needed. Quite a few mechanisms have been proposed to introduce such a E_F factor. (1) If DM halos have substructures, the local density can be enhanced so that the annihilation optical depth can be increased³¹⁹. Detailed N-body simulations, on the other hand, show that the boost factor intro-

duced by DM substructures is generally less than $E_F \sim 10$; (2) It is possible that DM in the early universe was not in equilibrium. In the scenarios of non-thermal production of DM, the interaction rate responsible for the e^\pm excesses are not directly related to the relic DM density. One may simply assume that the interaction rate is that required from the e^\pm excess data, and no boost factor is needed³²⁰; (3) More physically, there might exist new mediating particles during the DM annihilations. Examples include the Sommerfeld mechanism^{321,207} and the Breit-Wigner mechanism³²². The Sommerfeld mechanism³²¹ is a non-relativistic quantum mechanical effect. A large boost factor can be produced if DM interacts with a new light particle. Without such an interaction, annihilation of DM is a short distance effect. If DM interacts with a nearly massless (light) particle, then there is an additional long-range force (with Coulomb-like potential $V(r) = -b/r$), which would distort the DM wave-function before annihilation happens. This would introduce a modification factor to the annihilation cross section, so that $\sigma = \sigma^0 S$. The factor S is the Sommerfeld factor. By solving the non-relativistic Schrödinger equation, one can derive $E_F = S$. Assuming a dark matter particle χ coupling to a mediator ϕ with coupling strength λ , for S-wave annihilation in the nonrelativistic limit, one gets $E_F = (\pi b/v)/(1 - e^{-\pi b/v})$ for $m_\phi = 0$ and $E_F \leq \pi b m_{\text{dm}}/m_\phi$ for $m_\phi > 0$, where v is the velocity (in units of c) of each DM particle in the center-of-mass frame²⁰⁷. $E_F \sim 10^3$ is then achievable if $v \sim 10^{-3} b\pi$ for $m_\phi = 0$ or $m_{\text{dm}}/m_\phi \sim 10^3/b\pi$ for $m_\phi > 0$. The Breit-Wigner mechanism³²² applies to the case of a heavy mediating particle. For most masses of the mediating particle, the cross section is not enhanced. However, if the annihilation of DM is through the S-channel and if the new particle has a mass about twice of the DM mass, the cross section and annihilation rate can be greatly enhanced near a resonance point. This introduces a large enough E_F to interpret the data.

Another challenge the DM model faces in the e^\pm excess modeling is the non-detection of an excess in the antiproton spectrum⁵⁷. Contrary to the data, most DM annihilation models invoke a large hadronic annihilation fraction.

The requirement of having excesses only in e^\pm but not in anti-proton spectrum, along with the large boost factor needed as discussed above, pose great constraints and eliminate many candidate DM annihilation models. For example, the most popular DM candidate, the lightest supersymmetric particle (LSP) in the minimal supersymmetric standard model (MSSM) can give rise to the e^\pm excesses²⁰⁶. However, as a linear combination of photino, zino and higgsino, LSP usually has a large hadronic annihilation fraction, which is in conflict with the PAMELA anti-proton data. This model also suffers the problem of realizing a large boost factor. For the KK dark matter particles, direct annihilation to e^+e^- is possible. In fact, the lightest KK particles (LKP) was recognized²⁰⁰ as a potentially important source of positrons when the e^\pm excess was found by HEAT earlier. In the ATIC discovery paper²⁴, the KK models was also introduced as an example to account for the observed $e^+ + e^-$ spectrum peak around 600 GeV. These models again require a sig-

nificant fraction of annihilation in hadronic modes ($\sim 35\%$), which is at odds with the PAMELA antiproton data (cf. Ref.240). The required large boost factor E_F is attributed to halo sub-structures, which was found difficult to achieve. In the inert Higgs model, for a candidate with $m_{\text{dm}} \sim 70$ GeV, the DM annihilation contribution to e^+ and anti-proton fluxes is much smaller than the expected backgrounds. Even if a boost factor is invoked to enhance the signals, the particle candidate is unable to explain the observed e^+ and anti-proton data. Only a high mass candidate, with $m_{\text{dm}} \sim 10$ TeV, would be possible to fit the PAMELA excess provided a large enhancement, either in the local DM density or through the Sommerfeld effect³²³. Such a heavy particle, however, is in contradiction with the constraint from WMAP and various theoretical and experimental constraints¹⁸¹.

Recently two types of models have been constructed to account for the detection of the excess in the electron/positron channel but not in the antiproton channel (see Ref.27 for a recent review):

(1) The kinematically limited light particle decay models (e.g., Refs.207, 242, 243, 204, 244, 245, 246, 247, 248, 209, 249, 250, 251, 252, 253, 254, 255, 256, 257, 258, 259, 260, 261, 262); These models require the existence of a light particle with a mass less than the sum of proton and anti-proton masses. Such a low mass makes hadronic modes kinematically inaccessible and forces the particle decay predominantly into leptons. To accommodate the very high annihilation rate required to reproduce the current e^\pm excess, the light particle decay model makes use of its light force-carrier to generate the Sommerfeld enhancement²⁰⁷. For instance, in the MSSM extended by a singlet chiral superfield, the singlino-like neutralino dark matter annihilates to light singlet-like Higgs bosons, which proceed to decay to either electron-positron or muon-antimuon pairs. For the singlino-like neutralino dark matter with a mass ~ 2 TeV, PAMELA and Fermi data may be interpreted^{236,237}. Phenomenologically, the light particle decay can have multiple channels. For example, for the case of the mediating light particle being a light scalar ϕ ^{207,209}, for annihilation $\chi\chi \rightarrow \phi\phi$, one would consider four ϕ decay channels: 1) $\phi \rightarrow e^+e^-$, 2) $\phi \rightarrow \mu^+\mu^-$, 3) a mixture of 1:1 (or 2:1) between electrons and muons, and lastly 4) $\phi \rightarrow \pi^+\pi^-$ ²⁰⁹. Detailed modeling suggests that the models annihilating predominantly to μ are somewhat favored³²⁴. For the case of mediating light particle is a scalar s and a pseudoscalar a , i.e. $\chi\chi \rightarrow sa$, one has a also preferably decay to muons, i.e. $a \rightarrow \mu^+\mu^-$, and muons further decay to e^\pm detected on the Earth. Some spectrum modeling examples³²⁴ can be found in Fig.8, where the model N_3 is one of the Nomura-Thaler-type models²⁴⁴ and is characterized by $m_a = 0.8$ GeV and $m_s = 20$ GeV. The model AH_4 is one of the Arkani-Hamed et al.-type models²⁰⁷, in which the scalar dark matter particles annihilate into $\mu^+\mu^-$.

(2) The leptophilic DM models^{214,215,216,217,218}. These models can be realized by demanding DM interactions being leptophilic, namely, mediating DM particles only interact with the standard model leptons. The mediating particle does not have to be light. The only constraint on the mass comes from the requirement of sufficient

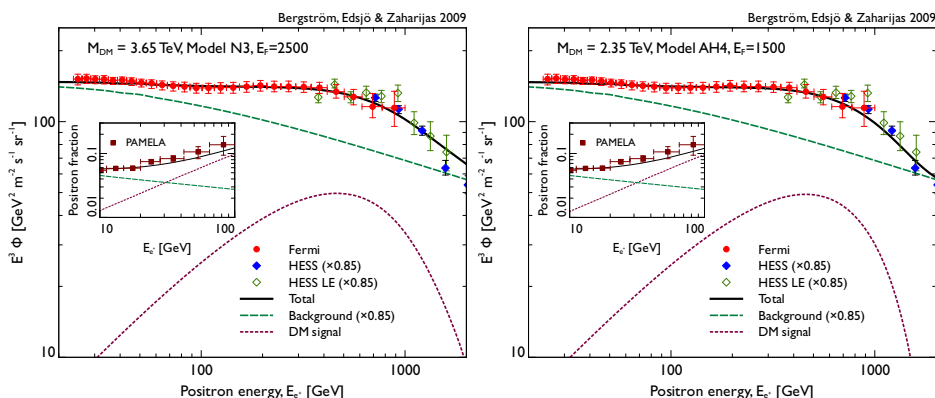


Fig. 8. Example spectra of good fit DM annihilation models found in Ref.324. The predicted $e^+ + e^-$ signal and background are compared against the Fermi and HESS data. The HESS data and the background model have been rescaled with a factor 0.85. In the inset, the positron fraction as measured by PAMELA is plotted against the predicted signal for the same model.

enhancement of the DM annihilation cross section. In the model with Sommerfeld enhancement the force-carrier particle should have a mass $\sim m_{\text{dm}}/E_F$, while in the model with Brei-Wigner enhancement the force-carrier particle should have a mass $\sim 2m_{\text{dm}}^{218}$.

The DM annihilation models, although most intensively discussed in the literature, are now facing strong observational and theoretical constraints. If the required boost factor $E_F \geq 10^3$ is not due to the DM substructures, and if one assumes such a boost and adopts a universal Navarro-Frenk-White (NFW) density profile of DM halos, a large annihilation γ -ray flux from nearby galaxy clusters is predicted. With the parameters that well fit the PAMELA and Fermi data³²⁴ and the standard assumptions for the limiting mass of the substructures within DM halos, it is found that the EGRET upper limit in γ -ray flux is violated in Virgo³²⁵. Similarly, the predicted gamma-ray flux violates the HESS upper limit constraints from the Galactic center and some dwarf spheroidals, and the predicted radio flux from synchrotron emission of the produced e^\pm from the Galactic Center also violates the current radio observation upper limits. The upper limits may be satisfied only if the DM density profile is significantly less steep than the benchmark NFW and Einasto profiles³²⁹. The diffuse γ -ray data from the Fermi first year observations have imposed a very tight constraint on the DM annihilation models and suggests that the annihilation models likely only work in some “fined-tuned” situations^{326,327}. From theoretical point of view, it is shown³²⁸ that the enhancement required in the Sommerfeld-enhanced DM annihilation models implies a thermal relic density that is too small to allow the DM candidate suitable for interpreting the e^\pm feature to account for all the DM in the universe. In Ref. 328 the authors also derived an upper bound on the possible Sommerfeld enhancements from the observations of elliptical galactic DM halos and showed that these bounds generically exclude such an explanation.

Counterarguments were also raised recently. It was argued³³⁰ that there are a lot of uncertainties in calculating the γ -ray signals from the nearby dwarf spheroidals and the Galactic Center, and that the annihilation models do not conflict with the Fermi gamma-ray limits. It was also found that the annihilation models are better than other models to account for the microwave signals collected by WMAP in the Galactic Center³³¹.

6.3.2. Dark matter decay models

The dark matter particles are often assumed to be perfectly stable as the result of a symmetry, e.g. R-parity in the supersymmetric models. However, from the gravitational evidence for the existence of dark matter we can only infer that dark matter has to be stable on timescales (much) longer than the age of the Universe. In other words, DM particles are allowed to decay. If they decay at a sufficiently high rate, the decay products might be detectable as cosmic rays, which would result in the observed e^\pm excess. There are in fact some physically well-motivated dark matter candidates that have very long lifetimes before decaying. For instance, gravitino dark matter, which is unstable due to a small breaking of the R-parity, constitutes an interesting scenario that leads to a thermal history of the universe consistent with the observed abundances of primordial elements, the observed dark matter relic abundance, and the observed baryon asymmetry¹⁷³. Some other decaying DM candidates discussed in the literature include hidden gauge bosons²⁸¹, hidden gauginos²⁸⁴, right-handed sneutrinos in R-parity breaking scenarios²⁸², KK dark matter in a simple extension of the minimal universal extra dimension models by introducing a small curvature³⁰⁶, and baryonic bound states of messenger quarks²⁸³. The late decay of dark matter particles, for example gravitinos, can produce gamma rays^{280,301}, positrons³³², neutrinos³³³ and/or antiprotons³³², which contribute to the total fluxes received at the Earth.

In the dark matter decay scenario(s), the source term of the electrons/positrons is given by

$$q(\vec{r}, p) = \frac{1}{\tau_{\text{dec}}} \frac{\rho_{\text{dm}, \odot}(\vec{r})}{m_{\text{dm}}} \frac{d\mathcal{N}_{e^\pm}}{d\mathcal{E}}, \quad (20)$$

where $\frac{d\mathcal{N}_{e^\pm}}{d\mathcal{E}}$ is the energy spectrum of the electrons/positrons produced by the decay of each DM particle. Evidently, in the decay model the parameters involved regarding the DM properties are the mass m_{dm} , the lifetime τ_{dec} , and the spectrum of decay, $\frac{d\mathcal{N}_{e^\pm}}{d\mathcal{E}}$.

In order to account for the excess in the electron/positron channel but not in the antiproton channel, the decay of DM should mainly produce leptons with suppressed hadronic branching ratios. As a result, the leptophilic decaying DM scenarios have attracted considerable attention. As in the annihilation scenarios, leptophilic decaying DM models can be broadly divided into two categories³³⁴. One is that DM first decays into some new light particles, which subsequently decay

into muons or electrons, while decays into hadrons are forbidden by kinematics. The other is that the DM particle couples mainly to leptons due to symmetry²⁸² or geometric setup³⁰⁶.

Although the decay models are not as widely investigated as the annihilating models, they have some advantages that are not shared by the annihilation models. First, in the decay models there is no need of the “boost factor” given the freedom of choosing the decay lifetime of the DM particles. Second, decay models suffer much less constraints from the gamma-ray and radio observations from the Galactic Center^{335,334,326}. Similar to the annihilation models, only the TeV e^\pm pairs generated within a distance ~ 1 kpc can reach us. In the popular NFW profile of the dark matter halo with $\rho(r) \propto r^{-1}$, one expects a much higher DM density near the Galactic Center. The gamma-ray signals produced in inverse Compton scattering off the star light and CMB by pairs produced in the Galactic Center can reach the Earth. Since the decay flux is proportional to the DM density ρ rather than proportional to ρ^2 as in the annihilation models, the decay models predict a much fainter signal than the annihilation models. The non-detection of such signals pose strong constraints on the annihilation models, but not the decay models (c.f. Ref.336, 330).

In the phenomenological approach, it is usually assumed that the dark matter particle is either a fermion (ψ_{dm}) or a scalar (ϕ_{dm}). Predictions for the positron fraction for various decay channels and different dark matter masses and lifetimes can be then computed^{284,337}. In the case of a fermionic dark matter particle, people usually consider the two-body decay channels $\psi_{\text{dm}} \rightarrow Z^0\nu$, $\psi_{\text{dm}} \rightarrow W^\pm\ell^\mp$, as well as the three-body decay channels $\psi_{\text{dm}} \rightarrow \ell^+\ell^-\nu$, with $\ell = e, \mu, \tau$ being the charged leptons. For a scalar dark matter particle, one usually considers the two-body decay channels $\phi_{\text{dm}} \rightarrow Z^0Z^0$, $\phi_{\text{dm}} \rightarrow W^+W^-$, and $\phi_{\text{dm}} \rightarrow \ell^+\ell^-$. In light of the PAMELA and Fermi data, some specific channels are found better than the others³³⁷. One example of spectral modeling is shown in Fig.9. The latest diffuse γ -ray data from Fermi first year observations excludes the dark matter decay model unless the dark matter decays mostly or even exclusively in $\mu^+\mu^-$ ³²⁶ (Fig.10, see however Refs. 327, 338 for looser constraints).

7. Discussions and Conclusions

After ~ 40 years of efforts, the cosmic ray electron/positron spectrum has been measured up to ~ 1 TeV/ ~ 100 GeV with an unprecedented accuracy. The rising of the positron-to-electron ratio above ~ 10 GeV, a tendency discovered in the 1970s⁴⁹, has been confirmed by the PAMELA satellite²¹ with high confidence. The electron + positron spectrum hardens above a few hundred GeV, as discovered by ATIC²⁴, PPB-BETS²⁵, Fermi-LAT²⁶ and HESS^{44,58}. The rising positron-to-electron ratio and the hardening electron + positron spectrum, unexpected in the standard cosmic ray model, are consistent with each other and are called e^\pm “excesses”. The detailed electron + positron spectral shape recorded by ATIC/PPB-BETS and Fermi/HESS are however different. Future more advanced experimental observations will pin

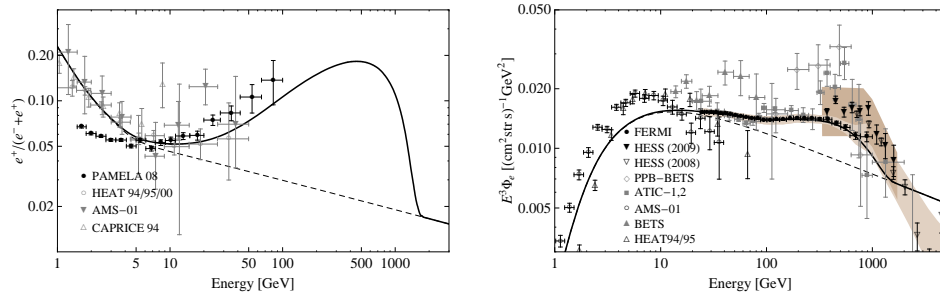
38 *Y. Z. Fan, B. Zhang & J. Chang*


Fig. 9. Positron fraction (*left panel*) and electron+positron flux (*right panel*) for the fermionic DM decay ($\psi_{\text{dm}} \rightarrow \mu^+ \mu^- \nu$) model. The parameters are $m_{\text{dm}} \sim 3.5$ TeV and $\tau_{\text{dec}} \sim 1.1 \times 10^{26}$ sec. The dashed line shows the astrophysical background. A scalar dark matter particle decay ($\phi_{\text{dm}} \rightarrow \mu^+ \mu^-$) model gives an equally well fit to the data for $m_{\text{dm}} \sim 2.5$ TeV and $\tau_{\text{dec}} \sim 1.8 \times 10^{26}$ sec. The figures are from Ref.337.

down the shape of the spectrum more accurately.

A lot of efforts have been made to interpret the observed electron/positron excesses. We summarize them in three main categories:

- In the standard cosmic ray model, the supernova remnants are the sole source of primary cosmic rays up to PeVs. The inhomogeneity of the supernova remnants^{66,67} and/or the secondary particle acceleration in supernova remnants^{79,80} may account for the PAMELA/ATIC/Fermi data. More speculatively, some physical processes taking place in young supernova remnants, for example, suppression of the high energy e^\pm cooling in the Klein-Nishina regime^{89,88} and e^\pm pair production by interactions between high-energy CRs and background photons⁸⁶, may also account for the observed excesses.
- It is possible that the observed e^\pm excesses originate from a new astrophysical CR source. The leading candidate is pulsars^{90,72,110}. Pulsars are known to be able to produce electron/positron pairs, which may be accelerated to the desired high energies outside the magnetospheres (likely in SNR shocks). No excess in the spectrum of antiproton cosmic rays is expected, in agreement with the PAMELA result. The escape of these pairs from the associated SNR, however, is unclear. One popular assumption is that pulsars should be mature, for which the associated SNR is too old to trap the pairs. The potential problem is that mature pulsars have lost a significant fraction of their initial kinetic energy and may not be powerful enough to reproduce the observations. Some other new astrophysical sources discussed in the literature include microquasars¹¹⁹ and local Gamma-ray Bursts¹³¹. The results are rather uncertain in these scenarios.
- The most extensively discussed interpretation of the e^\pm excesses is the annihilations or decays of dark matter. The excesses in positrons and antiprotons

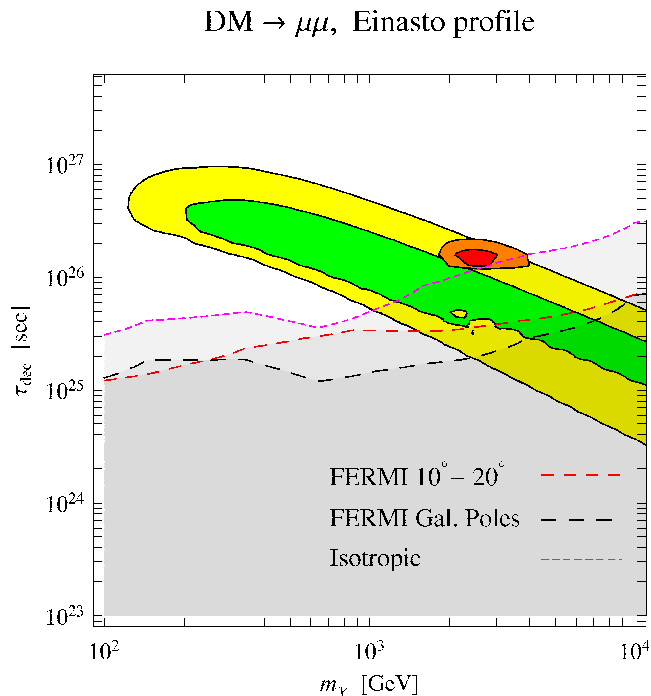


Fig. 10. The dark matter model parameter space $m_\chi - \tau_{\text{dec}}$ (dark matter mass–lifetime) and the constraints from the diffuse galactic gamma ray measurements by the Fermi satellite in its first year operation (from Ref.326). The exclusion contours are due to the Fermi observations of the ‘ $10^\circ - 20^\circ$ ‘strip’, the $|b| > 60^\circ$ ‘Galactic Poles’ region, and the isotropic flux, respectively. The regions allowed to fit the PAMELA positron data (green and yellow bands, 95% and 99.999% C.L. regions) and the PAMELA positron + Fermi and HESS data (red and orange blobs, 95% and 99.999% C.L. regions) in terms of decaying Dark Matter are also plotted.

in the CR spectra are two “standard” predictions of these models^{138,141}. The detection of a rising positron-to-electron ratio is a good news for these models. The non-detections of an excess in the antiproton spectrum, however, calls for modifications of most canonical dark matter models. Phenomenologically, one usually assumes that^{207,214,27,334} (1) the dark matter particles annihilate or decay into new particles, which are so light that can only finally decay into e^\pm and/or μ^\pm ; (2) the DM is leptophilic and couples only to leptons due to symmetry. In the DM annihilation models an unnatural large “boost factor” $\sim 10^3$ is needed to reproduce the PAMELA/ATIC/Fermi detected e^\pm fluxes. Such an unusually large boost factor is difficult to interpret simply by invoking substructures in the DM halo. Some particle-physics-oriented suggestions, such as the Sommerfeld and Briet-Wigner mechanisms, have been invoked to account for the large excess. Many specific models have emerged and are able to fit the elec-

tron/positron excesses. There are however some additional observational constraints. For example, almost all dark matter models predict a certain level excess of γ ray. The latest diffuse γ -ray data from the Fermi first year observations have excluded a large portion of the DM parameter space^{326,327,338}. (In contrast, the constraints on the astrophysical models are rather weak, since they are “local” phenomena and just occupy a small fraction of the volume of the Galaxy). In the case of annihilating DM, those models generating predominantly μ^\pm and assuming a cored Isothermal-like DM profile can fit the data with a mass $m_{\text{dm}} \sim 2$ TeV, but for other parameters, the model suffers various observational constraints and is less favored (c.f. Ref.330). In the case of decaying DM, again except those models generating predominantly μ^\pm (which can fit the data with $m_{\text{dm}} \sim 3$ TeV and $\tau_{\text{dec}} \sim 2 \times 10^{26}$ sec), most models are not favored by various observational constraints. It is worth noting that recently direct searches of dark matter have been performed by various experimental groups. For example, the CDMS II collaboration has observed two candidate events³³⁹. If interpreted as DM recoil on nuclei, the DM particles detected by CDMS II should be relatively light, with a mass $m_{\text{dm}} \sim \mathcal{O}(100)$ GeV. This is much lower than that needed in the e^\pm excesses modeling. Due to low statistics, it is of course too early to say that the observed e^\pm excesses are not of the DM origin. In any case, direct detection experiments and the high energy colliders (such as the Large Hadron Collider) would play an essential role to probe the nature of DM, and to provide a test to the current DM interpretations of the e^\pm excesses. In the near future, neutrino observations by the upcoming high energy neutrino detectors (such as IceCube) would also help to constrain the DM nature of the e^\pm excesses^{141,142}.

All the models reviewed here assume that the detected cosmic ray e^\pm excesses are due to one physical process. In reality, this may not be the case. For example, it is possibly that the detected excesses are mainly contributed by astrophysical processes, and the DM annihilation/decay signals are outshone. If so, the extraction of the DM properties via indirect detection experiments would be even more challenging. Nevertheless further indirect detection experiments are still necessary since they are complementary to the direct detection experiments and the collider experiments for revealing the properties of DM. For instance, collider experiments may identify a long-lived, weakly interacting particle and measure its mass. On the other hand, it would be difficult to test its cosmological abundance and stability. Such goals, however, are achievable in the direct and/or indirect detection experiments.

We conclude that both astrophysical processes and DM annihilation or decay models can provide a self-consistent explanation to the recently observed e^\pm excesses in the cosmic ray spectrum. At present the dark matter interpretations seem to be more exotic than some astrophysical scenarios. This is in particular the case for the dark matter annihilation models which are tightly constrained by the γ -ray

observational data by Fermi. In fact the latest diffuse gamma-ray data have excluded a large region of the DM parameter space that is favored in interpreting the e^\pm excesses. More experimental observations are needed to pin down the nature of DM and its implications for the e^\pm excess. Among the promising astrophysical models, the inhomogeneous distribution of supernova remnants has a smoking gun prediction that the positron-to-electron ratio is expected to decrease above an energy ~ 100 GeV. The pulsar model, instead, predicts an increasing positron-to-electron ratio up to the energy ~ 1 TeV. These two predictions will soon be tested by the ongoing PAMELA and the upcoming AMS-2 experiments. Both the inhomogeneous SNR model and the pulsar model predict a possible wiggle-like structure in the TeV energy range, which may be constrained by the observations of H.E.S.S.-like ground based Cherenkov telescopes.

Acknowledgements: This work is supported in part by the National basic research program of China under grant 2009CB824800 and a special grant of Chinese Academy of Sciences (for Y.Z.F), and by NASA NNX09AT66G, NNX10AD48G, and NSF AST-0908362 (for B.Z.) We thank P. H. Tam, Q. Yuan, X. J. Bi, and H. B. Hu for communications, and also D. Hooper for reading the manuscript.

References

1. V. L. Ginzburg, *Physics-Uspekhi*. **39**, 155 (1996).
2. J. Elster and H. Geitel, *Phys. Zs.* **2**, 560 (1901).
3. C. T. R. Wilson, *Camb. Phys. Soc. Proc.* **11**, 32 (1901).
4. C. T. R. Wilson, *Roy. Soc. Proc.* **68**, 151 (1901).
5. V. F. Hess, *Phys. Zs.* **13**, 1084 (1912).
6. W. Kolhorster, *Phys. Zs.* **14**, 1066 (1913).
7. V. L. Ginzburg and S. I. Syrovatskii, *The Origin of Cosmic Rays*. New York: Macmillan (1964)
8. P. Meyer, *Ann. Rev. Astron. Astrophys.***7**, 1 (1969).
9. P. Hillas, *Ann. Rev. Astron. Astrophys.***22**, 425 (1984).
10. M. Nagano and A. A. Watson, *Reviews of Modern Physics*. **72**, 689 (2000).
11. J. A. Earl, *Phys. Rev. Lett.***6**, 125 (1961).
12. P. Meyer and R. Vogt, *Phys. Rev. Lett.***6**, 193 (1961).
13. J. A. De Shong, R. H. Hildebrand and P. Meyer, *Phys. Rev. Lett.***12**, 3 (1964).
14. A. W. Strong, I. V. Moskalenko and V. S. Ptuskin, *Annu. Rev. Nucl. Part. Sci.* **57**, 285 (2007).
15. A. Buffington, C. D. Orth and G. F. Smoot, *Phys. Rev. Lett.***33**, 34 (1974).
16. R. R. Daniel and S. A. Stephens, *Phys. Rev. Lett.***15**, 769 (1965).
17. R. R. Daniel and S. A. Stephens, *Space Science Reviews*. **10**, 599 (1970).
18. B. Agrinier, *et al.*, *Lett. Nuovo Cimento*. **1**, 53 (1969).
19. D. Müller and K. K. Tang, *Astrophys. J.***312**, 183 (1987).
20. R. L. Golden, *et al.*, *Astron. Astrophys.***188**, 145 (1987).
21. O. Adriani *et al.* [PAMELA Collaboration], *Nature*.**458**, 607 (2009).
22. O. Adriani *et al.* [PAMELA Collaboration], *Astrophys. J.* submitted, arXiv:1001.3522 (2010).
23. R. J. Protheroe, *Astrophys. J.***254**, 391 (1982).
24. J. Chang *et al.* [ATIC Collaboration], *Nature*.**456**, 362 (2008).

42 Y. Z. Fan , B. Zhang & J. Chang

25. S. Torii *et al.*, arXiv:0809.0760 [astro-ph].
26. A. A. Abdo *et al.* [The Fermi LAT Collaboration], *Phys. Rev. Lett.***102**, 181101 (2009).
27. X. G. He, *Modern Physics Letters A.* **24**, 2139 (2009).
28. M. Boezio, *et al.*, *New Journal of Physics.* **11**, 105023 (2009).
29. C. L. Critchfield, E. P. Ney and S. Oleksa, *Phys. Rev.* **85**, 461 (1952)
30. B. Agrinier, Y. Koechlin and B. Parlier, *Phys. Rev. Lett.***13**, 377 (1964).
31. R. C. Hartman, *Astrophys. J.***150**, 371 (1967).
32. J. L. Fanelow, *et al.*, *Astrophys. J.***158**, 771 (1969).
33. R. L. Golden, *et al.*, *Astrophys. J.***436**, 769 (1994).
34. G. Barbiellini, *et al.*, *Astron. Astrophys.***309**, L15 (1996).
35. R. L. Golden, *et al.*, *Astrophys. J.***457**, L103 (1996).
36. S. W. Barwick, *et al.*, *Astrophys. J.***482**, L191 (1997); J. J. Beatty, *et al.*, *Phys. Rev. Lett.*, **93**, 241102 (2004).
37. M. Boezio, *et al.*, *Astrophys. J.***532**, 653 (2001).
38. J. J. Torii, *et al.*, *Astrophys. J.***559**, 973 (2001).
39. T. L. Cline, G. H. Ludwig and F. B. McDonald, *Phys. Rev. Lett.***13**, 786 (1964).
40. C. Y. Fan *et al.*, *Astrophys. J.***151**, 737 (1968).
41. G. M. Simment and F. B. McDonald, *Astrophys. J.***157**, 1435 (1969).
42. G. J. Hurford, *et al.*, *Astrophys. J.***192**, 541 (1974).
43. M. Aguilar *et al.* [AMS-01 Collaboration], *Phys. Lett. B.***646**, 145 (2007).
44. F. Aharonian *et al.* [H.E.S.S. Collaboration], *Phys. Rev. Lett.***101**, 261104 (2008).
45. K. C. Anand, R. R. Daniel and S. A. Stephens, *Phys. Rev. Lett.***20** 764 (1968)
46. D. Müller and P. Meyer, *Astrophys. J.***186**, 841 (1973).
47. G. Hartmann, D. Müller and T. Prince, *Phys. Rev. Lett.***38**, 1368 (1977).
48. K. K. Tang, *Astrophys. J.***278**, 881 (1984).
49. A. Buffington, C. D. Orth and G. F. Smoot, *Astrophys. J.***199**, 669 (1975).
50. J. Nishimura, *et al.*, *Astrophys. J.***238**, 394 (1980).
51. T. Kobayashi, *et al.*, *Proceedings of the 26th International Cosmic Ray Conference.* Vol. 3, 61 (1999).
52. K. C. Anand, R. R. Daniel and S. A. Stephens, *Proceedings of the 13th International Cosmic Ray Conference.* Vol. 1, 355 (1973).
53. J. A. Earl, D. E. Neely and T. A. Rygg, *J. Geophys. Res.* **77**, 1087 (1972).
54. C. A. Meegan and J. A. Earl, *Astrophys. J.***197**, 219 (1975).
55. J. J. Beatty, *et al.*, *Phys. Rev. Lett.***93**, 241102 (2004).
56. M. Boezio, *et al.*, *Adv. Spac. Res.* **27**, 669 (2001).
57. O. Adriani *et al.*, *Phys. Rev. Lett.***102**, 051101 (2009).
58. F. Aharonian *et al.* [H.E.S.S. Collaboration], *Astron. Astrophys.***508**, 561 (2009).
59. A. W. Strong and I. V. Moskalenko, *Astrophys. J.***509**, 212 (1998).
60. E. S. Seo and V. S. Ptuskin, *Astrophys. J.***431**, 705 (1994).
61. P. F. Yin *et al.*, *Phys. Rev. D.***79**, 023512 (2009).
62. M. Kamionkowski and M. S. Turner, *Phys. Rev. D.***43**, 1774 (1991).
63. E. A. Baltz and J. Edsjo, *Phys. Rev. D.***59**, 023511 (1999).
64. I. V. Moskalenko and A. W. Strong, *Astrophys. J.***493**, 694 (1998).
65. P. D. Serpico, *Phys. Rev. D.***79**, 021302 (2009).
66. N. J. Shaviv, E. Nakar and T. Piran, *Phys. Rev. Lett.***103**, 111302 (2009).
67. T. Piran, N. J. Shaviv and E. Nakar, 2009 (arXiv:0905.0904).
68. D. Grasso, *et al.*, *Astropart. Phys.* **32**, 140 (2009).
69. J. M. Jauch and F. Rohrlich, *The Theory of photons and Electrons*, 2nd Edition, Springer-Verlag, New York (1976).
70. T. Erber, *Rev. Mod. Phys.* **38**, 626 (1966).

71. I. Gebauer and W. de Boer, *Astron. Astrophys.* submitted (arXiv:0910.2027).
72. F. A. Aharonian, A. M. Atoyan, and H. J. Voelk, *Astron. Astrophys.* **294**, L41 (1995).
73. A. W. Strong and I. V. Moskalenko, *ICRC* **5**, 1964 (2001) [arXiv:astro-ph/0106505].
74. T. Kobayashi, Y. Komori, K. Yoshida, and J. Nishimura, *Astrophys. J.* **601**, 340 (2004).
75. A. M. Hillas, *J. Phys. G: Nucl. Part. Phys.* **31**, R95 (2005).
76. F. Aharonian, et al., *Astron. Astrophys.* **457**, 899 (2006).
77. C. K. Lacey and N. Duric, *Astrophys. J.* **560**, 719 (2001).
78. P. L. Biermann, J. K. Becker, A. Meli, W. Rhode, E. S. Seo and T. Stanev, *Phys. Rev. Lett.* **103**, 061101 (2009).
79. P. Blasi, *Phys. Rev. Lett.* **103**, 051104 (2009).
80. M. Ahlers, P. Mertsch and S. Sarkar, *Phys. Rev. D.* **80**, 123017 (2009).
81. D. Eichler, *Astrophys. J.* **237**, 809 (1980).
82. R. Cowsik, *Astrophys. J.* **241**, 1195 (1980).
83. P. Blasi and P. D. Serpico, *Phys. Rev. Lett.* **103**, 081103 (2009).
84. P. Mertsch and S. Sarkar, *Phys. Rev. Lett.* **103**, 081104 (2009).
85. G. R. Blumenthal, *Phys. Rev. D.* **1**, 1596 (1970).
86. H. B. Hu, Q. Yuan, B. Wang, C. Fan, J. L. Zhang, and X. J. Bi, *Astrophys. J.* **700**, L170 (2009).
87. G. B. Blumenthal and R. J. Gould, *Rev. Mod. Phys.* **42**, 237 (1970).
88. R. Schlickeiser and J. Ruppel, *New. J. Phys.*, **12**, 033044 (2010).
89. L. Stawarz, V. Petrosian and R. D. Blandford, *Astrophys. J.*, **710**, 236 (2010).
90. C. S. Shen, *Astrophys. J.* **162**, L181 (1970).
91. H. Yüksel, M. D. Kistler, and T. Stanev, *Phys. Rev. Lett.* **103**, 051101 (2009).
92. D. Hooper, P. Blasia, and P. D. Serpico, *J. Cos. Astropart. Phys.* **01**, 025 (2009).
93. R. N. Manchester, and J. H. Taylor, *Pulsars*, San Francisco: W. H. Freeman (1977)
94. A. A. Abdo et al. [The Fermi Collaboration], *Science* **325**, 840 (2009).
95. A. A. Abdo et al. [The Fermi Collaboration], *Astrophys. J. Supp.* **187**, 460 (2010).
96. M. A. Ruderman and P. G. Sutherland, *Astrophys. J.* **196**, 51 (1975).
97. V. V. Usov and D. B. Melrose, *Astrophys. J.* **464**, 306 (1996).
98. J. Arons, *Astrophys. J.*, **266**, 215 (1983).
99. J. K. Daugherty and A. K. Harding, *Astrophys. J.* **458**, 278 (1996).
100. B. Zhang and A. K. Harding, *Astrophys. J.*, **532**, 1150 (2000).
101. K. S. Cheng, C. Ho, and M. Ruderman, *Astrophys. J.* **300**, 500 (1986).
102. R. W. Romani, *Astrophys. J.* **470**, 469 (1996).
103. L. Zhang and K. S. Cheng, **487**, 370 (1997).
104. J. Arons and E. T. Scharlemann, *Astrophys. J.*, **231**, 854 (1979).
105. A. G. Muslimov, and A. K. Harding, *Astrophys. J.*, **588**, 430 (2003).
106. F. Pacini, *Nature* **216**, 567 (1967).
107. T. Gold, *Nature* **218**, 731 (1968).
108. J. P. Ostriker and J. E. Gunn, *Astrophys. J.* **157**, 1395 (1969).
109. D. Malyshev, I. Cholis and J. Gelfand, *Phys. Rev. D.* **80**, 063005 (2009).
110. S. Profumo, arXiv:0812.4457 (2009).
111. A. K. Harding and R. Ramaty, *ICRC* **2**, 92 (1987).
112. X. Chi, K. S. Cheng, and E. C. M. Young, *Astrophys. J.* **459**, L83 (1996).
113. L. Zhang and K. S. Cheng, *Astron. Astrophys.* **368**, 1063 (2001).
114. I. Busching, C. Venter, and O. C. de Jager, *Adv. Space Res.* **42**, 497 (2008).
115. A. M. Atoyan, F. A. Aharonian, and H. J. Völk, *Phys. Rev. D.* **52**, 3265 (1995).
116. Pohl, M. 2009, *Phys. Rev. D.* **79**, 041301 (2009).
117. I. F. Mirabel, L. F. Rodriguez, *Ann. Rev. Astron. Astrophys.* **37**, 409 (1999).
118. V. Bosch-Ramon and D. Khangulyan, *Int. J. Mod. Phys. D* **18**, 347 (2009).

119. S. Heinz and R. Sunyaev, *Astron. Astrophys.***390**, 751 (2002).
120. R. F. Fender, T. J. Maccarone, and Z. van. Kestern, *Mon. Not. R. Astron. Soc.***360**, 1085 (2005).
121. J. Albert, et al., *Science* **312**, 1771 (2006).
122. M. Tavani, et al., *Nature* **462**, 620 (2009).
123. N. Guessoum, P. Jean, and N. Prantzos, *Astron. Astrophys.*, **457**, 753 (2006).
124. R. W. Klebesadel, I. B. Strong, and R. A. Olson, *Astrophys. J.*, **182**, L85 (1973).
125. T. Piran, *Rev. Mod. Phys.*, **76**, 1143 (2004).
126. D. Guetta, T. Piran and E. Waxman, *Astrophys. J.*, **619**, 412 (2005).
127. B. Zhang and P. Mészáros, *Int. J. Mod. Phys. A*, **19**, 2385 (2004).
128. D. Frail, et al. *Astrophys. J.*, **562**, L55 (2001).
129. D. M. Coward, *Mon. Not. R. Astron. Soc.*, **360**, L77 (2005).
130. E. Liang, B. Zhang, F. Virgili, Z. G. Dai, *Astrophys. J.*, **662**, 1111 (2007).
131. K. Ioka, *Prog. Theo. Phys.* **123**, 743 (2010).
132. A. S. Fruchter, et al., *Nature*. **441**, 463 (2006).
133. S. Savaglio, K. Glazebrook, D. Le Borgne, *Astrophys. J.***691**, 182 (2009).
134. K. Z. Stanek et al. *Acta Astron.* **56**, 333 (2006)
135. P. D’Avanzo et al. *Astron. Astrophys.*, submitted (2010)
136. Y. Z. Fan and T. Piran, *Front. Phys. China.* **3**, 306 (2008).
137. J. L. Racusin, et al., *Nature*. **455**, 183 (2008).
138. G. Jungman, M. Kamionkowski and K. Griest, *Phys. Rept.* **267**, 195 (1996).
139. L. Bergström, *Rep. Prog. Phys.* **63**, 793 (2000).
140. C. Munoz, *Int. J. Mod. Phys. A*. **19**, 3093 (2004).
141. G. Bertone, D. Hooper and J. Silk, *Phys. Rept.* **405**, 279 (2005).
142. D. Hooper and S. Profumo, *Phys. Rept.* **453**, 29 (2007).
143. K. A. Olive, *Advances in Space Research.* **42**, 581 (2008).
144. F. D. Steffen, *The European Physical Journal C.* **59**, 557 (2009).
145. D. Hooper, (2009) [arXiv:0901.4090].
146. G. D’Amico, M. Kamionkowski and K. Sigurdson, arXiv:0907.1912 (2009).
147. L. Bergström, *New. J. Phys.* **11**, 105006 (2009).
148. U. Ellwanger, C. Hugonie, and A. M. Teixeira, arXiv:0910.1785 (2010).
149. J. L. Feng, *Ann. Rev. Astron. Astrophys.*, in press (arXiv:1003.0904)
150. F. Zwicky, *Helv. Phys. Acta* **6**, 110 (1933).
151. J. A. Peacock, *Cosmological Physics.*, Cambridge University Press, (1999).
152. F. Iocco, G. Mangano, G. Miele, O. Pisanti, and P. D. Serpico, *Phys. Rept.* **472**, 1 (2009).
153. K. G. Begeman, A. H. Broeils, and R. H. Sanders, *Mon. Not. R. Astron. Soc.***249**, 523 (1991).
154. R. D. Blandford and R. Narayan, *Ann. Rev. Astron. Astrophys.***30**, 311 (1992).
155. N. Bahcall and X. Fan, *Astrophys. J.***504**, 1 (1998).
156. D. N. Spergel et al. *Astrophys. J. Supp.* **148**, 175 (2003).
157. A. G. Riess et al. *Astron. J.* **116**, 1009 (1998).
158. E. Komatsu et al. *Astrophys. J.* submitted (2010) (arXiv:1001.4538).
159. D. J. Eisenstein et al. *Astrophys. J.***633**, 560 (2005).
160. C. Alcock et al. *Astrophys. J.***542**, 281 (2000).
161. T. Kikuchi and N. Okada, *Phys. Lett. B.***665**, 186 (2008).
162. A. Kusenko and M. E. Shaposhnikov, *Phys. Lett. B.***418**, 46 (1998).
163. ALEPH, DELPHI, L3, and OPAL Collaborations, *Phys. Lett.* **B565**, 61 (2003)
164. ALEPH, DELPHI, L3, and OPAL Collaborations,
http://lepewwg.web.cern.ch/LEPEWWG

165. J. Wess and B. Zumino, *Nucl. Phys. B.***70**, 39 (1974).
166. P. Fayet, *Phys. Lett. B.***86**, 272 (1979).
167. J. Ellis, J.S. Hagelin, D.V. Nanopoulos, K. Olive, M. Srednicki, *Nucl. Phys. B.***238**, 453 (1984).
168. H.E. Haber and G.L. Kane, *Phys. Rep.* **117**, 75 (1985).
169. T. Falk, K.A. Olive, and M. Srednicki, *Phys. Lett. B.***339**, 248 (1994).
170. C. Arina and N. Fornengo, *JHEP* **11**, 029 (2007).
171. J. L. Feng, A. Rajaraman, and F. Takayama, *Phys. Rev. Lett.***91**, 011302 (2003).
172. T. Moroi, H. Murayama, and M. Yamaguchi, *Phys. Lett. B.***303**, 289 (1993).
173. W. Buchmuller, L. Covi, K. Hamaguchi, A. Ibarra, and T. Yanagida, *JHEP* **0703**, 037 (2007).
174. W. Buchmuller, A. Ibarra, T. Shindou, F. Takayama, and D. Tran, *J. Cos. Astropart. Phys.***0909**, 021 (2009).
175. R. Peccei and H.R. Quinn, *Phys. Rev. Lett.***38**, 1440 (1977).
176. J. E. Kim and G. Carosi, *Rev. Mod. Phys.***82**, 557 (2010).
177. N. G. Deshpande and E. Ma, *Phys. Rev. D.***18**, 2574 (1978).
178. E. Ma, *Phys. Rev. D.***73**, 077301 (2006).
179. R. Barbieri, L. J. Hall and V. S. Rychkov, *Phys. Rev. D.***74**, 015007 (2006).
180. L. Lopez Honorez, E. Nezri, J. L. Oliver and M. H. G. Tytgat, *J. Cos. Astropart. Phys.***0702**, 028 (2007).
181. E. Dolle and S. F. Su, *Phys. Rev. D.***80**, 055012 (2009).
182. M. Gustafsson, E. Lundström, L. Bergström, and J. Edsjö, *Phys. Rev. Lett.***99**, 041301 (2007).
183. T. Goto and M. Yamaguchi, *Phys. Lett. B.***276**, 103 (1992).
184. S. A. Bonometto, F. Gabbiani, and A. Masiero, *Phys. Rev. D.***49**, 3918 (1994).
185. L. Covi, J.E. Kim, and L. Roszkowski, *Phys. Rev. Lett.***82**, 4180 (1999).
186. E. J. Chun, H. B. Kim, and D. H. Lyth, *Phys. Rev. D.***62**, 125001 (2000).
187. L. Covi and J.E. Kim, *New. J. Phys.* **11**, 105003 (2009).
188. P. Hut, *Phys. Lett.* **69B**, 85 (1977).
189. B.W. Lee and S. Weinberg, *Phys. Rev. Lett.***39**, 165 (1977).
190. M.I. Vysotsky, A.D. Dolgov and Ya. B. Zel'dovich, *JETP Lett.* **26**, 188 (1977).
191. J. E. Gunn, B.W. Lee, I. Lerche, D.N. Schramm and G. Steigman, *Astrophys. J.***223**, 1015 (1978).
192. Ch. Kraus et al. *Euro. Phys. J. C.* **40**, 447 (2005)
193. S. Tremaine and J.G. Gunn, *Phys. Rev. Lett.***42**, 407 (1979).
194. S. Dodelson and L. M. Widrow, *Phys. Rev. Lett.***72**, 17 (1994).
195. X. D. Shi and G. M. Fuller, *Phys. Rev. Lett.***82**, 2832 (1999).
196. K. N. Abazajian, arXiv:0903.2040 (2010).
197. A. Boyarsky, O. Ruchayskiy and M. Shaposhnikov, *Ann.Rev.Nucl.Part.Sci.* **59**, 191 (2009).
198. K. Abazajian, G. M. Fuller, and M. Patel, *Phys. Rev. D.***64**, 023501 (2001).
199. A. Boyarsky, J. Lesgourgues, O. Ruchayskiy, and M. Viel, *Phys. Rev. Lett.***102**, 201304 (2009).
200. H. C. Cheng, K. T. Matchev and M. Schmaltz, *Phys. Rev. D.***66**, 036005 (2002).
201. G. Servant and T. M. P. Tait, *Nucl. Phys. B.***650**, 391 (2003).
202. M. Cirelli and A. Strumia, *Nucl. Phys. B.***821**, 399 (2009).
203. V. Barger, W.Y. Keung, D. Marfatia, and G. Shaughnessy, *Phys. Lett. B.***672**, 141 (2009).
204. I. Cholis, L. Goodenough, D. Hooper, M. Simet, and N. Weiner, *Phys. Rev. D.***79**, 123505 (2009).

205. M. Cirelli, M. Kadastik, M. Raidal, and A. Strumia, *Nucl. Phys. B.***813**, 1 (2009).
206. L. Bergstrom, T. Bringmann, and J. Edsjo, *Phys. Rev. D* **78**, 103520 (2008).
207. N. Arkani-Hamed, D. P. Finkbeiner, T. Slatyer, and N. Weiner, *Phys. Rev. D.***79**, 015014 (2009).
208. M. Pospelov and A. Ritz, *Phys. Lett. B.***671**, 391 (2009).
209. I. Cholis, D. P. Finkbeiner, L. Goodenough, and N. Weiner, *J. Cos. Astropart. Phys.***0912**, 007 (2009).
210. D. A. Dicus, E. N. Kolb, and V. L. Teplitz, *Phys. Rev. Lett.***39**, 168 (1977).
211. A.J. Tylka, *Phys. Rev. Lett.***63**, 840 (1989).
212. M. S. Turner and F. Wilczek, *Phys. Rev. D.***42**, 1001 (1990).
213. E.A. Baltz and J. Edsjo, *Phys. Rev. D.***59**, 023511 (1999).
214. P. J. Fox and E. Poppitz, *Phys. Rev. D* **79**, 083528 (2009).
215. S. Baek and P. Ko, *J. Cos. Astropart. Phys.***0910**, 011 (2009).
216. H. S. Goh, L. J. Hall and P. Kumar, *JHEP* **0905**, 097 (2009).
217. H. Davoudiasl, *Phys. Rev. D.***80**, 043502 (2009).
218. X. J. Bi, X. G. He, and Q. Yuan, *Phys. Lett. B.***678**, 168 (2009).
219. J. Hisano, M. Kawasaki, K. Kohri and K. Nakayama, *Phys. Rev. D* **79**, 063514 (2009).
220. K. Ishiwata, S. Matsumoto and T. Moroi, *Phys. Lett. B* **675**, 446 (2009).
221. J. Kalinowski, S. F. King and J. P. Roberts, *JHEP* **0901**, 066 (2009).
222. R. Allahverdi, B. Dutta, K. Richardson-McDaniel and Y. Santoso, *Phys. Rev. D* **79**, 075005 (2009).
223. P. Grajek et al., *Phys. Rev. D.***79**, 043506 (2009).
224. J. H. Huh, J. E. Kim and B. Kyae, arXiv:0812.5004 [hep-ph].
225. I. Gogoladze, R. Khalid, Q. Shafi and H. Yuksel, *Phys. Rev. D.***79**, 055019 (2009).
226. B. Kyae, *J. Cos. Astropart. Phys.***0907**, 028 (2009).
227. R. Allahverdi, B. Dutta, K. Richardson-McDaniel and Y. Santoso, *Phys. Lett. B.***677**, 172 (2009).
228. R. C. Cotta, J. S. Gainer, J. L. Hewett and T. G. Rizzo, *New J. Phys.* **11**, 105026 (2009).
229. I. Gogoladze, R. Khalid and Q. Shafi, *Phys. Rev. D.***79**, 115004 (2009).
230. J. P. Hall and S. F. King, *JHEP* **0908**, 088, (2009).
231. M. Berg et al., *J. Cos. Astropart. Phys.***0908**, 035 (2009).
232. G. Belanger, F. Boudjema, A. Pukhov and R. K. Singh, *JHEP* **0911**, 026 (2009).
233. C. Liu, *Phys. Rev. D.***80**, 035004 (2009).
234. D. Feldman, Z. Liu, P. Nath and B. D. Nelson, *Phys. Rev. D.***80**, 075001 (2009).
235. D. A. Demir et al., *Phys. Rev. D.***81**, 030519 (2010).
236. D. Hooper and T. M. P. Tait, *Phys. Rev. D.***80**, 055028 (2009).
237. W. Wang, Z. Xiong, J. M. Yang and L. X. Yu, *JHEP* **0911**, 053 (2009).
238. Y. Bai, M. Carena and J. Lykken, *Phys. Rev. D.***80**, 055004 (2009).
239. Y. Bai and Z. Han, *Phys. Rev. D.***79**, 095023 (2009).
240. D. Hooper and K. M. Zurek, *Phys. Rev. D.***79**, 103529 (2009).
241. C. R. Chen et al., *JHEP* **0909**, 078 (2009).
242. M. Pospelov and A. Ritz, *Phys. Lett. B.***671**, 391 (2009).
243. A. E. Nelson and C. Spitzer, arXiv:0810.5167 [hep-ph].
244. Y. Nomura and J. Thaler, *Phys. Rev. D.***79**, 075008 (2009).
245. D. Feldman, Z. Liu and P. Nath, *Phys. Rev. D.***79**, 063509 (2009).
246. C. R. Chen, F. Takahashi and T. T. Yanagida, *Phys. Lett. B.***673**, 255 (2009).
247. T. Hur, H. S. Lee and C. Luhn, *JHEP* **0901**, 081 (2009).
248. M. Pospelov, *Phys. Rev. D.***80**, 095002 (2009).
249. L. Bergstrom et al., *Phys. Rev. D.***79**, 081303 (2009).

250. E. J. Chun and J. C. Park, *J. Cos. Astropart. Phys.***0902**, 026 (2009).
251. K. Hamaguchi, S. Shirai and T. T. Yanagida, *Phys. Lett. B.***673**, 247 (2009).
252. K. J. Bae et al., *Nucl. Phys. B.***817**, 58 (2009).
253. T. Gehrmann, N. Greiner and P. Schwaller, arXiv:0812.4240 [hep-ph].
254. L. Covi and J. E. Kim, *New J. Phys.* **11**, 105003 (2009).
255. R. Barbieri, L. J. Hall, V. S. Rychkov and A. Strumia, *J. Phys. G* **36**, 115008 (2009).
256. M. Ibe, Y. Nakayama, H. Murayama and T. T. Yanagida, *JHEP* **0904**, 087 (2009).
257. C. Cheung, J. T. Ruderman, L. T. Wang and I. Yavin, *Phys. Rev. D.***80**, 035008 (2009).
258. S. Cassel, D. M. Ghilencea and G. G. Ross, *Nucl. Phys. B.***827**, 256 (2010).
259. R. Essig, P. Schuster and N. Toro, *Phys. Rev. D.***80**, 015003 (2009).
260. K. Kohri, J. McDonald and N. Sahu, *Phys. Rev. D.***81**, 023530 (2009).
261. J. Mardon, Y. Nomura and J. Thaler, *Phys. Rev. D.***80**, 035013 (2009).
262. D. E. Morrissey, D. Poland and K. M. Zurek, *JHEP* **0907**, 050 (2009).
263. M. Cirelli, A. Strumia and M. Tamburini, *Nucl. Phys. B.***787**, 152 (2007).
264. E. Ponton and L. Randall, *JHEP* **0904**, 080 (2009).
265. K. M. Zurek, *Phys. Rev. D.***79**, 115002 (2009).
266. X. J. Bi, P. H. Gu, T. Li and X. Zhang, *JHEP* **0904**, 103 (2009).
267. S. Khalil, H. S. Lee and E. Ma, *Phys. Rev. D.***79**, 041701R (2009).
268. Q. H. Cao, E. Ma and G. Shaughnessy, *Phys. Lett. B.***673**, 152 (2009).
269. E. Nezri, M. H. G. Tytgat and G. Vertongen, *J. Cos. Astropart. Phys.***0904**, 014 (2009).
270. D. J. Phalen, A. Pierce and N. Weiner, *Phys. Rev. D.***80**, 063513 (2009).
271. F. Chen, J. M. Cline and A. R. Frey, *Phys. Rev. D.***79**, 063530 (2009).
272. P. H. Frampton and P. Q. Hung, *Phys. Lett. B.***675**, 411 (2009).
273. M. Cirelli and A. Strumia, *New J. Phys.* **11**, 105005 (2009).
274. A. A. El-Zant, S. Khalil and H. Okada, arXiv:0903.5083 [hep-ph].
275. J. H. Huh, J. E. Kim and B. Kyae, *Phys. Rev. D.***80**, 115012 (2009).
276. I. Gogoladze, N. Okada and Q. Shafi, *Phys. Lett. B.***679**, 237 (2009).
277. W. L. Guo and X. Zhang, *Phys. Rev. D.***79**, 115023 (2009).
278. X. Calmet and S. K. Majee, *Phys. Lett. B.***679**, 267 (2009).
279. P. H. Gu, H. J. He, U. Sarkar and X. m. Zhang, *Phys. Rev. D.***80**, 053004 (2009).
280. A. Ibarra and D. Tran, *Phys. Rev. Lett.***100**, 061301 (2008).
281. C. R. Chen, F. Takahashi and T. T. Yanagida, *Phys. Lett. B.***671**, 71 (2009).
282. C. R. Chen and F. Takahashi, *J. Cos. Astropart. Phys.***0902**, 004 (2009).
283. K. Hamaguchi, E. Nakamura, S. Shirai and T. T. Yanagida, *Phys. Lett. B.***674**, 299 (2009).
284. A. Ibarra and D. Tran, *J. Cos. Astropart. Phys.***0902**, 021 (2009).
285. C. R. Chen, M. M. Nojiri, F. Takahashi and T. T. Yanagida, *Prog. Theor. Phys.* **122**, 553 (2009).
286. E. Nardi, F. Sannino and A. Strumia, *J. Cos. Astropart. Phys.***0901**, 043 (2009).
287. K. Ishiwata, S. Matsumoto and T. Moroi, *Phys. Rev. D.***79**, 043527 (2009).
288. M. Pospelov and M. Trott, *JHEP* **0904**, 044 (2009).
289. J. Hisano, M. Kawasaki, K. Kohri and K. Nakayama, *Phys. Rev. D.***79**, 043516 (2009).
290. J. Liu, P. F. Yin and S. H. Zhu, *Phys. Rev. D.***79**, 063522 (2009).
291. F. Takahashi and E. Komatsu, arXiv:0901.1915 [astro-ph].
292. C. H. Chen, C. Q. Geng and D. V. Zhuridov, *Phys. Lett. B.***675**, 77 (2009).
293. K. Hamaguchi, F. Takahashi and T. T. Yanagida, *Phys. Lett. B.***677**, 59 (2009).
294. X. Chen, *J. Cos. Astropart. Phys.***0909**, 029 (2009).
295. K. J. Bae and B. Kyae, *JHEP* **0905**, 102 (2009).

296. R. Essig, N. Sehgal and L. E. Strigari, *Phys. Rev. D.*, 023506 (2009).
297. S. Shirai, F. Takahashi and T. T. Yanagida, *Phys. Lett. B.***675**, 73 (2009).
298. K. Ishiwata, S. Matsumoto and T. Moroi, *JHEP* **0905**, 110 (2009).
299. M. Endo and T. Shindou, *JHEP* **0909**, 037 (2009).
300. S. L. Chen, R. N. Mohapatra, S. Nussinov and Y. Zhang, *Phys. Lett. B.***677**, 311 (2009).
301. K. Ishiwata, S. Matsumoto and T. Moroi, arXiv:0903.3125 [hep-ph].
302. A. Ibarra, A. Ringwald, D. Tran and C. Weniger, *J. Cos. Astropart. Phys.***0908**, 017 (2009).
303. A. Arvanitaki et al., *Phys. Rev. D.***80**, 055011 (2009).
304. S. Shirai, F. Takahashi and T. T. Yanagida, *Phys. Lett. B.***680**, 485 (2009).
305. C. H. Chen, C. Q. Geng and D. V. Zhuridov, arXiv:0905.0652 [hep-ph].
306. N. Okada and T. Yamada, *Phys. Rev. D.***80**, 075010 (2009).
307. H. Fukuoka, J. Kubo and D. Suematsu, *Phys. Lett. B.***678**, 401 (2009).
308. C. H. Chen, arXiv:0905.3425 [hep-ph].
309. L. Zhang, G. Sigl and J. Redondo, *J. Cos. Astropart. Phys.***0909**, 012 (2009).
310. C. H. Chen, C. Q. Geng and D. V. Zhuridov, *J. Cos. Astropart. Phys.***0910**, 001 (2009) [arXiv:0906.1646].
311. D. Aristizabal Sierra, D. Restrepo and O. Zapata, *Phys. Rev. D.***80**, 055010 (2009).
312. J. H. Huh and J. E. Kim, *Phys. Rev. D.***80**, 075012 (2009).
313. D. G. E. Walker, arXiv:0907.3142 [hep-ph].
314. H. Murayama and J. Shu, *Phys. Lett. B.***686**, 162 (2010).
315. W. Buchmuller et al., *J. Cos. Astropart. Phys.***0909**, 021 (2009).
316. J. N. Bahcall and R. M. Soneira, *Astrophys. J. Suppl.* **44**, 73 (1980).
317. J. F. Navarro, C. S. Frenk and S. D. M. White, *Astrophys. J.***462**, 563(1996).
318. B. Moore et al., *Mon. Not. R. Astron. Soc.***310**, 1147 (1999).
319. J. Lavalle, Q. Yuan, D. Maurin and X. J. Bi, *Astron. Astrophys.***479**, 427 (2008).
320. B. Dutta, L. Leblond and K. Sinha, *Phys. Rev. D.***80**, 035014 (2009).
321. A. Sommerfeld, *Annalen der Physik* **403**, 257 (1931).
322. M. Lattanzi and J. I. Silk, *Phys. Rev. D.***79**, 083523 (2009).
323. E. Nezri, M. H. G. Tytgat, and G. Vertongen, *J. Cos. Astropart. Phys.***0904**, 014 (2009).
324. L. Bergstrom, J. Edsjo, and G. Zaharijas, *Phys. Rev. Lett.***103**, 031103 (2009).
325. A. Pinzke, C. Frommer, and L. Bergström, *Phys. Rev. Lett.***103**, 181302 (2009).
326. M. Cirelli, P. Pancic, P. D. Serpico, (arXiv:0912.0663).
327. M. Papucci and A. Strumia, (arXiv:0912.4504).
328. J. L. Feng, M. Kaplinghat, H. B. Yu, *Phys. Rev. Lett.***104**, 151301 (2010).
329. G. Bertone, M. Cirelli, A. Strumiac, and M. Taoso, *J. Cos. Astropart. Phys.***0903**, 009 (2009).
330. G. Hütsi, A. Hektor, and M. Raidal, JCAP, submitted, arXiv:1004.2036 (2010)
331. T. Lin, D. Finkbeiner, and G. Dobler, arXiv:1004.0989 (2010)
332. A. Ibarra and D. Tran, *J. Cos. Astropart. Phys.***0807**, 002 (2008).
333. L. Covi, M. Grefe, A. Ibarra, and D. Tran, *J. Cos. Astropart. Phys.***0901**, 029 (2009).
334. C. R. Chen, S. K. Mandal, and F. Takahashi, *J. Cos. Astropart. Phys.***1001**, 023 (2010).
335. J. Liu, Q. Yuan, X. J. Bi, H. Li, and X. M. Zhang, (arXiv:0911.1002).
336. D. Hooper, A. Stebbins, and K. M. Zurek, *Phys. Rev. D.***79**, 103513 (2009).
337. A. Ibarra, D. Tran, and C. Weniger, *J. Cos. Astropart. Phys.***1001**, 009 (2010).
338. L. Zhang, C. Weniger, L. Maccione, J. Redondo, and G. Sigl, (arXiv:0912.4504).
339. Z. Ahmed, et al., (arXiv:0912.3592).